Microphysical Modeling of Cloud Droplet Activation over Dominica

Rick Russotto
Advisor: Trude Storelvmo
Second Reader: Ronald B. Smith
Submitted April 27, 2012

A Senior Thesis presented to the faculty of the Department of Geology and Geophysics, Yale University, in partial fulfillment of the Bachelor's Degree.

Abstract

The process of cloud droplet activation, in which aerosol particles become nuclei for cloud droplets, is essential for our understanding of the impacts of aerosols on Earth's climate because of the effects of aerosol concentration on the albedo and lifetime of clouds. The 2011 Dominica Experiment (DOMEX) field campaign provides an interesting opportunity to test existing models of droplet activation and growth in a tropical, orographic, convective setting; these data include aerosol and cloud droplet concentrations and size distributions, and wind speed measurements, from research flights above and upwind of the island of Dominica. This study involves modeling experiments using the Abdul-Razzak and Ghan parameterization of droplet activation, which is commonly used in regional and global climate models, as well as cloud-resolving models, but here is used as a standalone model. The model is run with inputs based on data from DOMEX, including aerosol size distribution data from the source air for the clouds, and updraft velocity data taken during cloud penetrations. The cloud droplet concentrations predicted by the model are compared with droplet concentration observations from DOMEX to see if the model results are reasonable. We run various experiments, such as changing the criterion for cloud penetrations or shifting aerosol size distribution toward larger or smaller sizes, both to try to resolve the discrepancies between model results and observations and to identify the changes to which the model results are most sensitive. We find that it is particularly important to have a good knowledge of the size distribution of particles smaller than 0.1 μm, as well as the mean in-cloud updraft velocity, in order to predict the fraction of activated aerosols. These findings should be useful to researchers interested in cloud microphysics who are planning future observational campaigns in similar environments.

Contents

1. Introduction

The process of cloud droplet activation, in which aerosol particles become nuclei for the water droplets that make up liquid water clouds, is an important process essential for our understanding of the impacts of aerosol particles and clouds on Earth's weather and climate. The concentration, composition, and size distribution of aerosols in the source air play a major role in determining the concentration and size distribution of cloud droplets. A higher aerosol concentration, for example, would result in more, smaller droplets forming from the same amount of condensed water vapor. This would make the cloud more brightly reflective to incoming solar shortwave radiation, thus reducing the amount of shortwave radiation reaching the surface and acting to reduce the surface temperature. Also, a higher number of cloud droplets would take longer to grow to the sizes needed for precipitation to occur, thus increasing the lifetime of the cloud. A cloud may have a net cooling or warming effect on the surface depending on its location and time of day, and a longer cloud lifetime would enhance whichever effect the cloud already has on the surface temperature. On a global average, however, longer cloud lifetimes would have a net cooling effect on the surface temperature.

A large fraction of aerosol particles in modern times are emitted into the atmosphere by humans, and the effect of these changes on clouds constitutes an anthropogenic forcing on Earth's climate. The effects of changes in aerosols on cloud shortwave reflectivity and cloud lifetime have been referred to as the first and second aerosol indirect effects, respectively (e.g. by [*Ramaswamy et al.*, 2001]), or as the cloud albedo effect and cloud lifetime effect (e.g. by *Lohmann and Feichter* [2005]). These effects are among the most uncertain components of the human impact on Earth's climate [*Forster et al.*, 2007].

In order to effectively simulate the aerosol indirect effects, global climate models (GCMs) must simulate the process of cloud droplet activation. Since actually resolving these processes is currently too computationally expensive for GCMs—most have a grid scale too large even to resolve clouds—it is necessary to handle the process instead with simple parameterizations that estimate the activation fraction (the fraction of aerosol particles that become cloud droplet nuclei) using analytical expressions based on the basic controlling factors, which include aerosol composition and size distribution, and the rate at which the clouds cool (determined by updraft velocity). *Ghan et al.* [2011] provide a good summary of the parameterizations used in various GCMs and other weather and climate models.

The recently completed Dominica Experiment (DOMEX) field campaign, described in detail in the "Observations" section (Section 2) below, provides an interesting opportunity to test the performance of droplet nucleation parameterizations in a tropical, island, orographic setting, and to use droplet activation models in conjunction with the observations to study the process of cloud droplet activation in this setting. One of the most commonly used droplet nucleation parameterizations is that developed by *Abdul-Razzak et al.* [*Abdul-Razzak and Ghan*, 2000; *Abdul-Razzak et al.*, 1998], hereafter referred to as the ARG model.[1] Here, aerosol size distribution and updraft velocity data collected during DOMEX are used to run the ARG model, and the resulting cloud droplet concentration (the estimated activation fraction multiplied by the input aerosol concentration) is compared to the in situ observations made using the CDP and FSSP instruments.

Many of the important input parameters were not extensively measured during DOMEX (such as composition), or otherwise have high uncertainty (such as updraft velocity), and since the ARG parameterization has previously been shown to work well in many situations [*Ghan et al.*, 2011], any discrepancies between the model results and observations are far more likely due to the assumptions made in this study than to an inability of the model to perform well in a tropical, orographic environment. However, looking at the sensitivity of the model results to various assumptions used, or to changes to the major input parameters on the order of the level of uncertainty, can provide insights into which factors are important in determining the droplet activation fraction in this setting. This should be useful to those planning future observational campaigns, by illuminating what needs to be measured in order to adequately simulate cloud droplet activation in models.

[1] I use the words "parameterization" and "model" interchangeably when referring to this parameterization; the reader should not attempt to draw a distinction. Both terms are appropriate in a sense: while it is a parameterization used to handle cloud droplet activation in larger models, it is also being used in this study as a kind of crude dynamical model to study cloud droplet activation in the context of the DOMEX campaign.

2. Observations: The DOMEX Field Campaign

The Dominica Experiment (DOMEX) is a recently completed field campaign intended to study the physics and dynamics of orographic clouds in a tropical island setting. In April and May 2011, 21 research flights were flown over the island of Dominica and the surrounding ocean using the University of Wyoming King Air research aircraft. The campaign and its major initial conclusions are described in [*Smith et al.*, 2012]. This is a summary of the flights and instrumentation of the campaign, and those findings in *Smith et al* relevant to this study.

2.1 Flight Paths

Figure 1 depicts the topography of the island and defines the flight legs along which data were taken, and Figure 2 shows an example flight path. A typical DOMEX flight would take off from Martinique, where the aircraft was based, and travel northward toward Dominica, flying up to 4000 m as it did so. The aircraft would then descend to 150 m in order to obtain a vertical profile of atmospheric conditions. These would be followed by Legs 1, east of the island, and 2, just off the east coast, at altitudes of 300 and 1200 m each. Next, the aircraft would fly Legs 3 and 4, above the mountainous spine of the island, once, twice, or three times each, at an

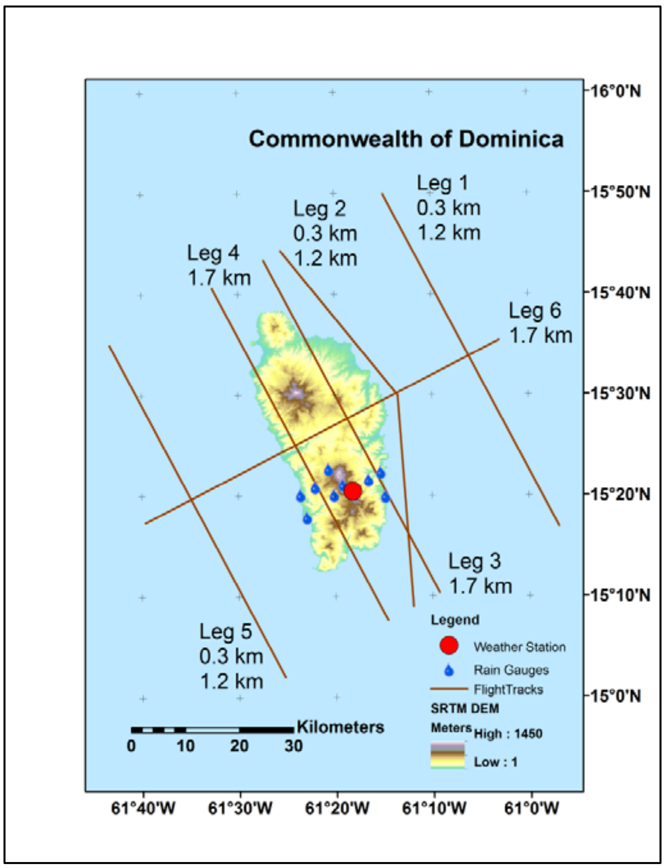

Figure 1. Topography of the island of Dominica; definition of research flight legs (including altitude); and locations of ground observations. From *Smith et al.* [2012].

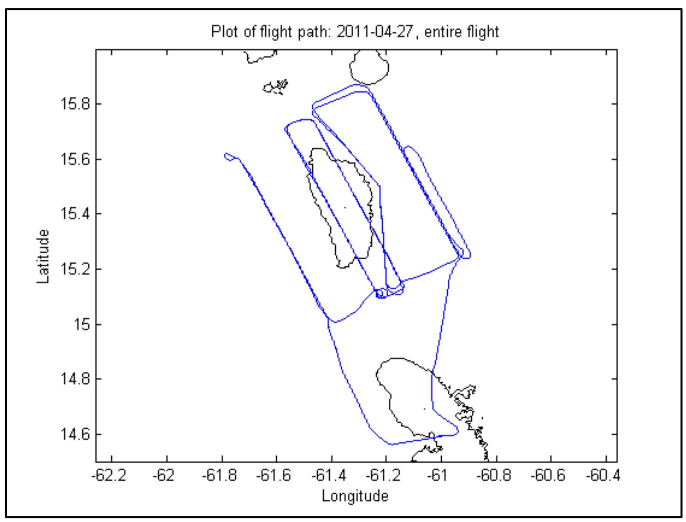

Figure 2. Flight path of RF13, a typical DOMEX flight, flown April 27, 2011. This flight included two versions each of legs 3 and 4, and leg 5 at 300 and 1200 m, but not leg 6.

altitude of 1700 m. Then, typically either Leg 5, off the west coast of Dominica, or Leg 6, perpendicular to the north-south axis of the island, would be flown before returning to Dominica.

Dominica, at roughly 15°30” N latitude, is in the trade wind regime, meaning that the prevailing surface winds are from the east. Therefore, under normal conditions, Legs 1 and 2 are upwind of the island, and Leg 5 is downwind of the island.

2.2 Instruments

The Wyoming King Air carried numerous instruments to make various cloud physics-related measurements. These included optical particle counters to make *in situ* measurements of the concentrations and size distributions of aerosol particles, cloud droplets and raindrops in the air passed through by the aircraft; other instruments to measure variables like humidity, liquid water content (LWC), temperature, and carbon dioxide concentration; and radar and lidar systems to measure cloud particles and aerosol particles, respectively, above and below the aircraft.

The instruments most relevant to cloud droplet activation are the optical counters that measured the concentrations and size distributions of aerosol particles and cloud droplets *in situ*. This study makes use of four such instruments, which are summarized in Table 1.

Table 1: DOMEX Aerosol and Cloud Droplet Instruments

Instrument	CN counter	PCASP	FSSP	CDP
Measures:	Aerosols	Aerosols	Cloud droplets	Cloud droplets
Size Range (μm)	> 0.01	0.095-2.99	2-47	2-50
Size Bins?	No	Yes	Yes	Yes
Mechanism	Butanol saturation; internal optical system	Dried particles; internal optical system	External optical system	External optical system

The CN counter detects aerosol particles larger than 0.01 μm in diameter. It saturates the particles with butanol and then counts the number of times a laser beam is interrupted by the saturated particles. This can be used to obtain the number concentration of particles per unit volume, if the sample volume and the air flow velocity through the beam are also known. (The other particle counters work according to similar principles.) This instrument does not provide any information on the size distribution of the particles, but detects smaller particles than any other instrument on board.

The Passive Cavity Aerosol Spectrometer Probe (PCASP) uses an optical system to determine the concentration and size distribution of aerosol particles from 0.095 to 2.99 μm in diameter. This instrument removes any condensed water from the particles before measuring them. The boundaries of the size bins for this instrument are given in Appendix A. For particles with diameters similar to the laser wavelength of 0.6328 μm, Mie scattering effects become important in determining the apparent size of the particle; this effect is dependent on the particle index of refraction. The PCASP was calibrated using latex beads with an index of refraction of 1.588, but aerosols in the field often have lower indices of refraction, so the particle diameters may actually be larger than the nominal diameter for nominal diameters between about 0.1 μm and 1 μm [*Liu and Daum*, 2000].

The Forward Scattering Spectrometer Probe (FSSP) is an external optical particle counter intended for measuring cloud droplets, with diameters from 2 to 47 μm. It measures both concentration and size distribution. The Cloud Droplet Probe (CDP) is a newer version of the FSSP which measures roughly the same information (particles from 2 to 50 μm). Comparing the results from the two redundant instruments can provide some insight into the uncertainty of the measurements. These instruments can also be used to determine the liquid water content, in g m^{-3}.

2.3 <u>Initial Findings of Campaign: Dynamical Regimes</u> (see [*Smith et al.*, 2012])

DOMEX was intended to study the dynamics of tropical orographic precipitation in situations in which convection is triggered by forced ascent of air over a ridge due to strong horizontal flow (i.e. strong trade winds). However, much of the observation period was characterized by unusually weak trade winds, sometimes less than 3 m/s for Leg 1L. This led to the identification of two dynamical regimes by *Smith et al.*, called the "low wind case" and the "high wind case". Figure 3 shows a schematic of these two regimes.

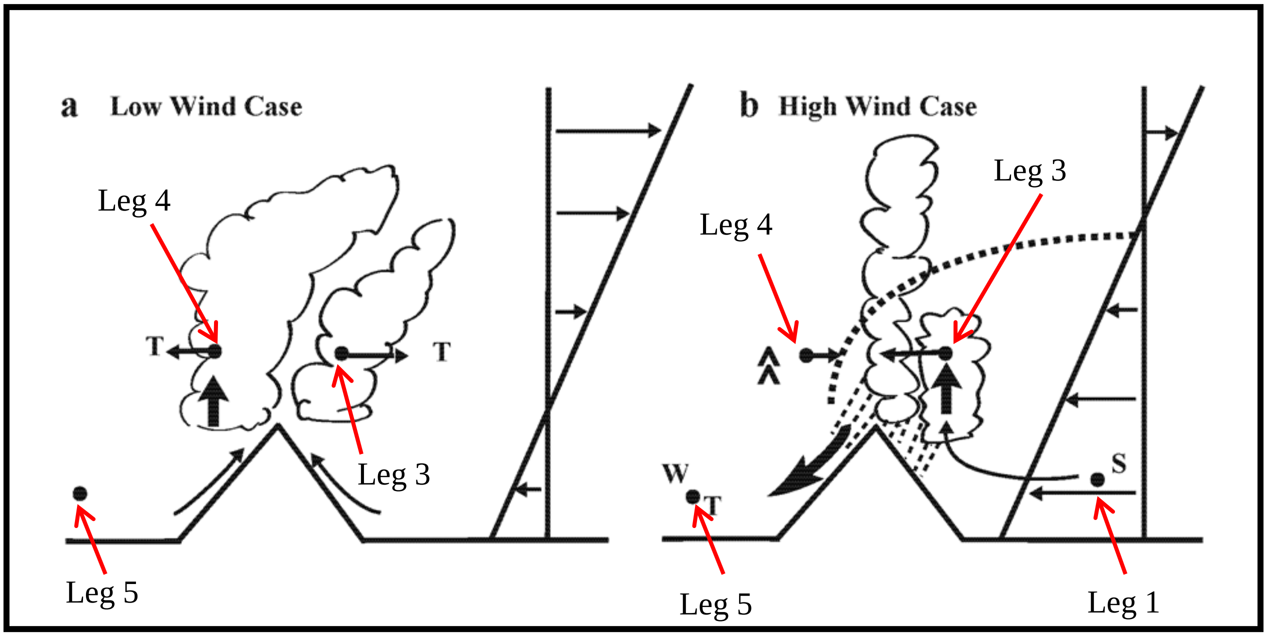

Figure 3. Schematic of low and high wind convection regimes. Trade wind vertical profiles are shown to the right of the island; thin curved arrows show the source air for the clouds. Circular dots show flight legs, which are annotated; convection is strongest over Leg 3 for the high wind case, and Leg 4 for the low wind case. From [*Smith et al.*, 2012]

In the low wind case, convection is forced by diurnal heating of the island surface (thermally driven convection). For the low wind case, island-derived aerosols are advected upward as the source air for the clouds rises along the slopes of the mountains. Many of these island-derived particles act as cloud condensation nuclei, resulting in higher droplet concentrations, smaller droplets, and less precipitation relative to the high wind case, in which island-derived aerosols are absent and total aerosol concentrations are lower. The low-wind case is marked by diverging air high above the island, which brings island-derived aerosols out over the ocean upstream from the island.

The high wind case is the regime which the campaign was designed to study; in this regime, convection cells form as horizontally moving air is forced upward over the mountains (mechanically driven convection). For the high wind case, the source air for the clouds never comes in contact with the island, and contains primarily marine-derived aerosols. The mechanism which is thought to be responsible for the high-wind convection is the "lapse rate mechanism" [*Kirshbaum and Smith*, 2009; *Woodcock*, 1960]: pre-existing clouds—or air with high relative humidity, which will form clouds first—in the upstream air will ascend at the moist adiabatic lapse rate while the surrounding, drier air will rise at the dry adiabatic lapse rate[2]. This makes the moister incoming parcels warmer than their surroundings, resulting in positive buoyancy anomalies which become the cores of the convective cells.

Evidence for the origin of the cloud air comes from CO_2 measurements: for the low wind flights, CO_2 is depleted in the portions of Legs 3 and 4 over the island, where the clouds are, relative to the portion over the ocean to the north and south. For the high wind flights, however, the air in the clouds over the island does not show CO_2 depletion. CO_2 depletion implies contact with vegetation. Therefore, these observations indicate that the air in the clouds has been in contact with the island for the low wind days but not the high wind days. [*Smith et al.*, 2012]

Table 2 lists the horizontal wind speed and direction as well as other variables for Leg 1L for the 21 research flights. Flights RF07 and RF08 are considered to represent the low wind case, and RF12, RF13, RF16, and RF17 represent the high wind case. RF09 was not counted in the low wind flights, despite wind speeds comparable to RF07 and RF08, because it lacked the diverging air aloft characteristic of the low wind case. RF01 was not counted in the high wind flights, despite high wind speed, because flight clearance issues prevented most of the legs from being flown below an altitude of 2100 m.

[2] The adiabatic lapse rate is the rate in K/m at which an air parcel will cool if lifted adiabatically (without heat transfer into or out of the parcel). The "moist" and "dry" adiabatic lapse rates refer to this rate when condensation does and does not occur, respectively. The dry adiabatic lapse rate is about 9.8 K/km. The moist adiabatic lapse rate is lower, typically around 6 K/km (but temperature dependent), due to latent heat release; this difference is the basis for moist convection in the atmosphere.

Table 2: DOMEX research flights: Upstream conditions at 300m (Leg 1L) (From [*Smith et al.*, 2012])						
RF #	Date	Wind Speed	Wind Direction	Temperature	Relative Humidity	Class
Units		m/s	degrees	°C	%	
1	5 April	9.7	85	24.4	70.4	
2	8 April	*				
3	9 April	7.6	76	23.9	70.5	
4	10 April	6.0	89	23.9	77.9	
5	14 April	4.4	98	24	87.7	
6	15 April	4.6	110	24.1	86	
7	18 April	3.4	25	23.7	77.5	LW
8	19 April	2.7	58	23.9	76.5	LW
9	21 April	3.0	131	24.3	73	
10	24 April	5.6	90	24.8	79	
11	25 April	7.8	92	24.6	78	
12	26 April	10.1	90	24.9	76.9	HW
13	27 April	11.4	82	24.5	80.8	HW
14	28 April	**				
15	30 April	7.7	97	24.7	78.5	
16	1 May	9.7	83	24	83.2	HW
17	2 May	9.2	79	24.6	80.5	HW
18	3 May	7.3	83	24.8	79.7	
19	4 May	5.7	102	24.2	84.8	
20	6 May	**				
21	7 May	8.5	88	23.4	98.1	

(* aborted flight; **heavy rain upwind, LW=low wind regime; HW-high wind regime)

3. Model: The Abdul-Razzak *et al*. Parameterization

Three different papers describe different versions of the aerosol activation parameterization used in this study. *Abdul-Razzak et al.* [1998] describe the simplest version of the model, which considers only aerosols with a size distribution described by a single lognormal mode[3], and which has uniform internally mixed composition[4]. The version used in this study is the second version, described in *Abdul-Razzak and Ghan* [2000], which considers multiple lognormally distributed aerosol modes, each of which can have a different internally mixed composition. In the last version, described in *Abdul-Razzak and Ghan* [2002], the aerosol size distribution is represented by a number of different size bins, with a uniform concentration and internally mixed chemical composition of particles in each bin; this is called a "sectional representation" and allows for treatment of size distributions that diverge widely from lognormal distributions. All references to the parameterization hereafter refer to the multiple lognormal mode version. This section provides a condensed description of what the parameterization calculates, what inputs are required to run it, and how the calculation is performed.

The parameterization considers a parcel of initially cloud-free air, rising adiabatically[5] at constant speed. It is used to calculate the maximum supersaturation[6] reached in the parcel as it rises, and hence the fraction of activated aerosol, assuming that the maximum supersaturation is the critical supersaturation[7] for the smallest particle activated in each mode, which should be the case if the chemical composition in each mode is homogeneous and the particles are all spherical. The model inputs, described below, include information on the size distribution for each mode; the hygroscopicity of the particles in each mode[8]; and the spectrum of updraft velocities.

---

[3] A lognormal distribution is a distribution that appears as a normal distribution when the x-axis is plotted on a log scale; see below for the mathematical form.

[4] Internally mixed composition means that to the extent that different chemical species are present, they are found within the same particles in a constant ratio.

[5] This means that there is no heat transfer into or out of the parcel (excluding latent heat release due to condensation).

[6] Supersaturation is the relative humidity minus one, where the relative humidity is the ratio of the partial pressure of water vapor to the saturation vapor pressure with respect to a flat gas-liquid interface. The saturation vapor pressure is the pressure at which the liquid and gas phases of water are at equilibrium in a closed system.

[7] The critical supersaturation is the supersaturation at which a given particle will become activated, meaning that the condensed water droplet forming around it will begin unstable growth.

[8] Hygroscopicity is the ability of the particles to attract water molecules; more hygroscopic particles make better condensation nuclei.

3.1 Model Inputs

Each mode's size distribution is described by a lognormal distribution, the form of which can be represented by:

$$n(a) = \frac{N_t}{\sqrt{2\pi}\ln\sigma}\exp\left[-\frac{\ln^2(\frac{a}{a_m})}{2\ln^2\sigma}\right] \tag{1}$$

where n is the aerosol number size distribution in cm^{-3} μm^{-1}; a is the particle diameter (or radius); N_t is the total aerosol number concentration in cm^{-3}; a_m is the geometric mean diameter (or radius) for the mode, which for lognormal distributions is, conveniently, equal to the median diameter; and σ is the geometric standard deviation (which is dimensionless) for the mode. Thus there are three parameters, N_t, a_m, and σ, which define the aerosol size distribution for each mode. These can be estimated based on CN and PCASP data; this process is described in the "Defining Model Inputs" section (Section 4) below.

The chemical composition of the aerosol modes is taken into account via a hygroscopicity parameter, B, which is used in defining critical supersaturation as a function of radius for each mode (the more hygroscopic the particles, the lower the critical supersaturation for a given radius). For a single aerosol type in one mode, the hygroscopicity parameter is calculated as follows:

$$B = \frac{\nu\varphi\epsilon M_w\rho_a}{M_a\rho_w} \tag{2}$$

where ν is the number of ions the salt portion of the aerosol type dissociates into; φ is the osmotic coefficient, which describes the deviation of the solution from ideal solvent behavior (ideal meaning that the intermolecular forces between the solute and solvent are no stronger than those between solvent molecules); ϵ is the solubility, or the fraction of the aerosol material that is soluble (which would be 1 for simple salts like sodium chloride or ammonium sulfate, but < 1 for more complex materials like mineral dust); M_w is the molecular weight of water; M_a is the molecular weight of the dry aerosol; ρ_w is the density of water; and ρ_a is the density of the dry aerosol. This means that the chemistry for each species of aerosol present is expressed using five parameters: ν, φ, ϵ, M_a, and ρ_a. For multiple internally mixed chemical species in a single mode, the values of ν, φ, ϵ, M_a, and ρ_a, and the mass fraction for each aerosol type are used to calculate a single hygroscopicity parameter for the mode.

In order to account for the variability of updraft velocity within the turbulent, convective clouds, a Gaussian spectrum of updraft velocities is considered; the mean and standard deviation updraft velocities $\overline{w}$ and σ_w must be provided in order to run the model. The activation fraction is calculated 200 times for a parcel with different updraft velocities. Where updraft velocity is negative, the activation fraction is assumed to be 0. The total activation fraction returned is an average of the results for the 200 updraft velocities, weighted according to the Gaussian probability density function (PDF) with the given values of $\overline{w}$ and σ_w.

In summary, running the model requires specifying the number of lognormal modes; N_t, a_m, and σ for each mode; ν, φ, ϵ, M_a, and ρ_a for each aerosol type; the mass fraction of each aerosol type for each mode; and the mean and standard deviation of the updraft velocity distribution. In addition, the temperature and density of air at the cloud base must also be specified; these are used to calculate constants used in the parameterization, but the dependence of the results on these variables is weak [*Ghan et al.*, 2011].

3.2 How the Parameterization Works[9]

The parameterization assumes that the fraction of activated aerosols for each mode is equal to the fraction of aerosols larger than the smallest activated aerosol for that mode. According to the Köhler theory of droplet activation, the critical supersaturation of an aerosol particle is a function of its radius:

$$S' = \frac{2}{\sqrt{B}}\left(\frac{A}{3a}\right)^{3/2} \tag{3}$$

where a is the dry particle radius, A is a coefficient of the effect of droplet curvature on the saturation vapor pressure of water at its surface, and B is the hygroscopicity parameter defined in (2). A and B are constants for a mode so S' is a function only of a. A particle will become activated if the supersaturation ever exceeds its critical supersaturation; therefore, if the maximum supersaturation the parcel undergoes as it rises is known, equation (3) can be used to find the radius of the smallest particle activated for the mode. Thus the problem of finding the activation fraction can be reduced to a problem of finding the maximum supersaturation as the parcel rises.

[9] This is a condensed version including only those equations necessary to understand the basic operating principles of the parameterization. For a more complete mathematical description see [*Abdul-Razzak et al*, 1998] and [*Abdul-Razzak and Ghan*, 2000].

The supersaturation of an air parcel as it rises can be expressed as

$$\frac{dS}{dt} = \alpha V - \gamma \frac{dW}{dt} \tag{4}$$

where S is the supersaturation; α and γ are size-invariant coefficients; V is the updraft velocity; and W is the liquid water content in kg m^{-3}. The αV term represents the effect of the cooling of the parcel due to adiabatic expansion as it rises, which lowers the saturation vapor pressure of water, increasing the supersaturation, and the $-\gamma \frac{dW}{dt}$ term represents the effect of the removal of water vapor by the growing droplets. The maximum supersaturation can be found by setting dS/dt equal to 0 in equation (4) and solving.

The condensation rate can be expressed as

$$\frac{dW}{dt} = 4\pi\rho_w \int_0^S r^2 \frac{dr}{dt}\, n(S')\, dS' \tag{5}$$

where *r(S,S')* is the droplet radius as a function of *S(t)*, the supersaturation, and *S'*, the critical supersaturation for the particle.[10] *n(S')* is the particle number size distribution expressed in terms of *S'* instead of dry particle radius (see equation (3)). The integral with respect to *S'* ensures that growth is being considered for all particles that have been activated at time *t*—that is, all particles with a critical supersaturation *S'* less than or equal to the actual supersaturation *S* at time *t*. The equation for the droplet growth rate is

$$\frac{dr}{dt} = \frac{G}{r}\left(S - \frac{A}{r} + \frac{Ba^3}{r^3}\right) \tag{6}$$

where G is a growth coefficient which, due to gas kinetic effects, is dependent on r; A/r represents the curvature effect; and Ba^3/r^3 represents the hygroscopicity effect.

It is not mathematically possible to solve for the maximum supersaturation using equations (5) and (6) substituted into equation (4), unless some simplifying assumptions are made. In this parameterization, this is done by neglecting the curvature, hygroscopicity, and size dependence of G—thus neglecting gas kinetic effects—in equation (6) (but the curvature effect is accounted for again later by the addition of a nondimensional parameter ζ). Then an

[10] The Köhler curve describes droplet size as a function of supersaturation for a given particle, taking the curvature and solution effects into account; it is used to derive equation (3). With the constants *A* and *B* known, *S'* is a function only of the dry particle radius. *S'* then determines the shape of the Kohler curve for a particular droplet, and *S(t)* determines the droplet radius at time *t*.

approximation is made assuming that for small particles, growth before activation is dominant, and for large particles, growth after activation is dominant; this allows for the droplet radius to be eliminated from the rate equations, and for the coefficients to be re-expressed in terms of two dimensionless parameters, η and ζ, defined below:

$$\eta = \frac{(\alpha V/G)^{3/2}}{2\,\pi\,\rho_w\,\gamma\,N_t} \tag{7}$$

$$\zeta = \frac{2}{3}\left(\frac{\alpha V}{G}\right)^{1/2} A \tag{8}$$

An expression can then be derived which determines the maximum supersaturation:

$$S_{\max} = \frac{1}{\left\{\sum_{i=1}^{I} \frac{1}{S_{mi}^2}\left[f_i\left(\frac{\zeta}{\eta_i}\right)^{3/2} + g_i\left(\frac{S_{mi}^2}{\eta_i + 3\zeta}\right)^{3/4}\right]\right\}^{1/2}} \tag{9}$$

where I is the number of modes; S_{mi} is the critical supersaturation for a particle with the median radius for mode i; f_i and g_i are constants defined as follows:

$$f_i \equiv 0.5\exp(2.5\,\ln^2\sigma_i) \tag{10}$$

$$g_i \equiv 1 + 0.25\,\ln(\sigma_i) \tag{11}$$

where σ_i is the geometric standard deviation for the mode.

Equation (9) is an approximate analytical expression for the maximum supersaturation in terms of 4 dimensionless parameters for each mode, S_{mi}, σ_i, η_i, and ζ, allowing the maximum supersaturation, and hence the droplet activation fraction for each mode, to be computed very quickly. This makes the parameterization very suitable for use in GCMs, and it has also been used in a number of regional climate models and cloud-resolving models (*Ghan et al* [2011] provide a summary).

3.3 Limitations of Parameterization

Since droplet radii are eliminated from the rate equations in the derivation of equation (9), the parameterization provides only the activation fraction for each mode, and no information on the size distribution of the activated droplets. Other assumptions or calculations are needed to get this information. Some GCMs simply assume that the activated droplets from each mode have a certain size distribution at the time of maximum supersaturation. The National Center for Atmospheric Research (NCAR) Community Atmosphere Model, Version 5 (CAM5), for example, assumes that activated droplets have a gamma distribution [*Morrison and Gettelman*, 2008].

Also, the parameterization does not consider entrainment of dry air into a cloud, which can lower the water vapor concentration and reduce the number of activated droplets. In cumulus clouds, this means that the parameterization would be expected to perform better in the center of the clouds than at the edges, where turbulent mixing brings dry air into the cloud; that hypothesis is tested in this study.

Finally, neglecting gas kinetic effects in the growth coefficient G can allow large droplets, whose growth is limited by the ability of water vapor to reach the droplet, to grow faster than they should. This leads to an underestimation of the activation fraction in situations where kinetic limitations are significant, because in reality the water vapor that cannot reach the larger droplets is available to allow other droplets to grow. Kinetic limitations are most important in situations with low updraft velocities, high aerosol number concentrations, and large aerosol particle diameters, and tend to be more important for anthropogenic aerosols than for pristine marine aerosols [*Nenes et al.*, 2001].

4. Defining Model Inputs

This section describes the general methodology by which the parameters used to run the ARG model are chosen. Where specific examples, figures, etc. are given, they are for the high wind "standard run" assumptions, the justifications for which are given here. The modeling results for the high wind standard runs, and comparison to observations, are described in Section 5.1. Tests of the sensitivity of the model results to various assumptions of the standard run are described in Section 5.2-5.8. A model run for the low wind cases is described in Section 6. See Section 3.2 for a description of how the model uses the inputs defined here.

4.1 Aerosol Size Distribution

Information on the aerosol size distributions can be obtained from the CN and PCASP data (see Section 2.2) averaged over the flight legs corresponding to the source air for the clouds. For the high wind cases, the air in the clouds comes from the altitudes between legs 1L (300 m) and 1H (1200 m), so for the "standard run" the CN and PCASP data used are averaged first over the individual legs and then between the low and high versions of the leg. To filter out possible inflated particle concentrations due to cloud penetrations or rain, data taken while the CDP- or FSSP-derived liquid water content exceeded 0.003 g m^{-3} (a conservative criterion) are not included in leg averages.

The PCASP size distribution extends down only to 0.095 nm, while the CN counter counts particles as small as 0.01 nm but does not record size distributions. By subtracting the total PCASP particle concentration from the CN particle concentration, an additional "bin" representing particles from 0.01 to 0.095 nm in diameter can be created. Thus we create a combined observed particle size distribution from the data from the two instruments. The parameters a_m, σ, and N_t can be determined by fitting lognormal distributions to parts of this distribution; that process is described here.

Figure 4 shows the combined CN and PCASP size distribution for RF12, one of the high wind flights, on a log-log scale. Three distinct maxima are apparent, one being the CN bin, and the other two in the PCASP bins at about 0.14 and 0.6 μm. These correspond to three different lognormal modes, referred to hereafter as the "Aitken mode", the "accumulation mode", and the "coarse mode", respectively. While no fourth maximum is present in this figure, we found that for the high wind cases, using only three modes significantly underestimated the concentrations in the very largest PCASP bins, so a fourth mode, the "giant mode", was added to account for this. Hereafter, $a_{m,A}$, $a_{m,ac}$, $a_{m,c}$, and $a_{m,g}$ refer to the median diameter for the Aitken, accumulation, coarse and giant modes, respectively, with a similar notation for σ and N_t.

The lack of information on size distribution between 0.01 and 0.095 µm, where the Aitken mode is located, means that the median diameter $a_{m,A}$ and geometric standard deviation σ_A for that mode must be estimated based on the literature. In the CAM-Oslo GCM, an extension of the NCAR CAM3 model, the Aitken mode for sea salt is assumed to have a median diameter of 0.044 µm and a geometric standard deviation of 1.59 [*Seland et al.*, 2008]. However, using 0.044 µm for $a_{m,A}$ resulted in the Aitken mode lognormal distribution overestimating some of the smallest PCASP bin concentrations, which would imply a negative concentration for the overlapping accumulation mode. So, $a_{m,A}$ was changed to 0.040 µm. The sensitivity of the model results to changes of this magnitude is tested in Section 5.4.

With values assumed for $a_{m,A}$ and σ_A, a probability density function (PDF) for the Aitken mode size distribution is

$$n(a) = \frac{1}{\sqrt{2\pi}\,\ln\sigma_A} \exp\left[-\frac{\ln^2(\frac{a}{a_{m,A}})}{2\ln^2\sigma_A}\right] \tag{12}$$

This is equivalent to equation (1) divided by N_t. $n(a)$ can be integrated over diameters from 0.01 to 0.095 µm; since the area under the PDF is 1, this integral is the fraction of the Aitken mode particles with sizes between the boundaries for the CN bin. Then, $N_{t,A}$ is the CN bin concentration divided by this fraction.

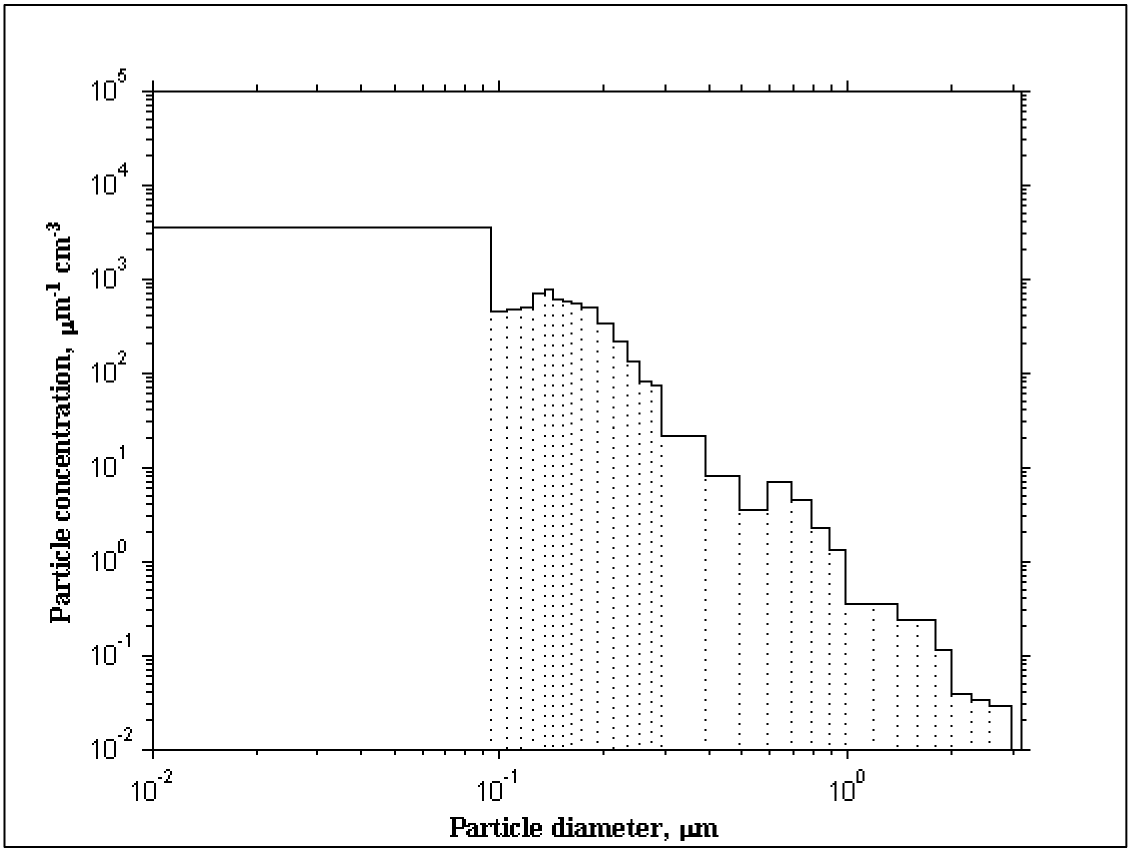

Figure 4. Combined observed particle size distribution from CN and PCASP, in particles cm^{-3} μm^{-1}, for RF12, an example high wind flight. Axes on log scale. Data shown are an average of the leg averages from Legs 1L and 1H. Dotted lines show bin boundaries. Leftmost “bin” from CN, all others from PCASP (see Appendix A for PCASP bin boundaries).

The accumulation mode parameters are calculated using PCASP bins 1-16, with diameters ranging from 0.095-0.491 μm. Since the same particles should not be counted twice in different modes, the Aitken mode concentration in each of these bins (found by numerically integrating equation (12) between the bin’s boundaries, and multiplying by the Aitken mode number concentration $N_{t,A}$) is subtracted from the PCASP particle concentration for the bin. Any negative values of this modified PCASP size distribution are set to 0 (using 0.040 μm for the Aitken mode median diameter avoids most occurrences of this). Then, $N_{t,ac}$ is calculated by summing the modified bin concentrations for bins 1-16.

The median diameter $a_{m,ac}$ is calculated by finding the lowest-numbered bin for which the cumulative sum of PCASP bin concentrations exceeds $0.5*N_{t,ac}$, then interpolating between the bin boundaries according to:

$$a_{m,ac} = \mathrm{UB}_{n-1} + (\mathrm{UB}_n - \mathrm{UB}_{n-1}) * \left(\frac{0.5 * N_{t,ac} - \mathrm{CS}(n-1)}{\mathrm{CS}(n) - \mathrm{CS}(n-1)}\right) \tag{13}$$

where n is the index of the PCASP bin that contains the diameter $a_{m,ac}$; UB_i is the upper bound size of the PCASP bin with index i (see Appendix A); and CS(i) is the cumulative sum of PCASP bin concentrations through bin i.

One way to find the geometric standard deviation σ for a lognormal mode is to first find the diameter $a*$ below which 84.1% of the particles lie; the geometric standard deviation is equal to the ratio of $a*$ to a_m [*Seinfeld and Pandis*, 2006]. We calculate $a*_{ac}$ using a similar methodology to $a_{m,ac}$:

$$a^*{}_{ac} = \mathrm{UB}_{m-1} + (\mathrm{UB}_m - \mathrm{UB}_{m-1}) * \left(\frac{0.841 * N_{t,ac} - \mathrm{CS}(m-1)}{\mathrm{CS}(m) - \mathrm{CS}(m-1)}\right) \tag{14}$$

where m is the index of the PCASP bin that contains the diameter $a*_{ac}$.

For the coarse mode, $N_{t,c}$, $a_{m,c}$, and σ_c are calculated using the same methods as for the accumulation mode, but using PCASP bins 17-29, from 0.491 to 2.991 μm. The Aitken mode concentration is negligible at these sizes, and the overlap between the accumulation and coarse modes is assumed to be negligible for the purposes of calculating the lognormal fit parameters for these two modes.

For the giant mode, only PCASP bins 23-29 (1.191-2.991 μm) are used. The coarse mode concentration in each of these bins is calculated by numerical integration based on the previously calculated $N_{t,c}$, $a_{m,c}$, and σ_c, and these concentrations are subtracted from the total bin concentrations to create a modified size distribution for the giant mode. Then, this modified size distribution is used to calculate $N_{t,g}$, $a_{m,g}$, and σ_g, using methods similar to those used for the accumulation and coarse modes.

Figure 5 shows, on a log-log scale, the lognormal distribution curves for the four modes superimposed over the observed particle size distribution from Figure 4. Table 2 shows the 12 lognormal fit parameters (N_t, a_m, and σ for the four modes) assumed or calculated for RF12, the flight shown in Figures 4 and 5. The sum of the fitted modes matches the observed distribution fairly well, except below 0.095 µm, for which there is only one bin, and above about 1 µm, where data is noisy due to low particle concentrations. No obvious changes are apparent that would improve the fits.

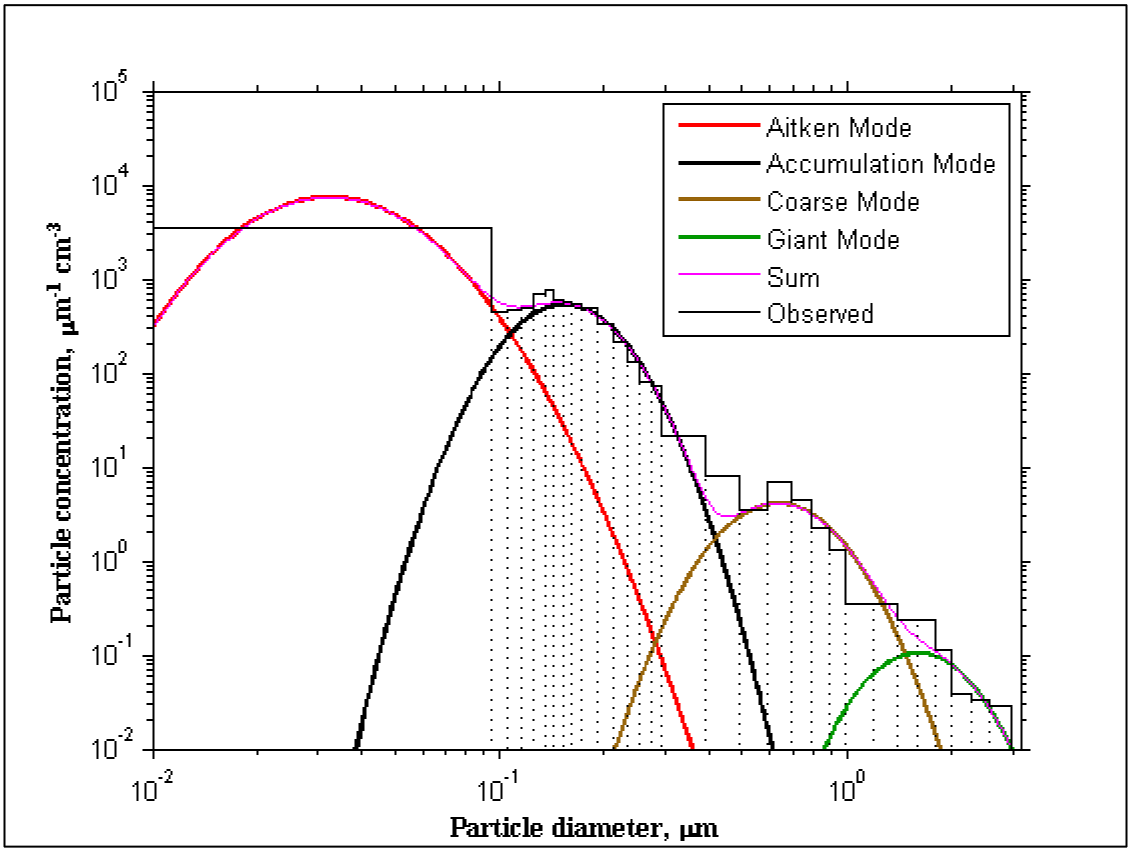

Figure 5. Figure 4 with calculated aerosol number concentrations for the four lognormal modes. "Sum" refers to the sum of the four calculated modes, and should, ideally, match the "observed" stepwise curve, which shows the size distribution from CN and PCASP.

Table 3: Lognormal distribution fit parameters for RF12, Legs 1L and 1H averaged			
Mode	Number concentration, N_t (cm^{-3})	Median diameter, a_m (μm)	Geom. st. dev., σ (dimensionless)
Aitken	309.1659	0.0400*	1.5900*
Accumulation	63.0903	0.1675	1.3446
Coarse	2.1259	0.6973	1.3653
Giant	0.1262	1.7398	1.3333

*$a_{m,A}$ and σ_A were assumed rather than calculated from the data.

4.2 Aerosol Composition

PCASP and particle volatility observations from the Rain In Cumulus over the Ocean (RICO) campaign, which was conducted upwind of Barbuda, in the Lesser Antilles, from November 2004-January 2005, showed that aerosols smaller than 0.2 μm in diameter were composed mainly of ammonium sulphate, and those larger than 0.2 μm were composed mainly of sea salt [*Peter et al.*, 2008]. Since these data were taken under conditions similar to the DOMEX upstream leg on high wind days, it is reasonable to assume that the DOMEX high wind source aerosol composition would be similar to that from RICO.

This would suggest that for running the ARG model, the Aitken mode should be entirely ammonium sulphate; the coarse and giant modes should be entirely sea salt; and the accumulation mode should be mainly ammonium sulphate but also include some sea salt, since 0.2 μm is below the 0.491 μm boundary between the bins used to calculate the accumulation and coarse modes. For the sake of simplicity, however, the accumulation mode is assumed to consist entirely of ammonium sulphate.

Table 4 gives the parameters v, φ, ϵ, M_a, and ρ_a used to calculate the hygroscopicity parameter B for ammonium sulfate and sea salt (see equation (2) in Section 3.1), as well as the values of B itself. These values are taken from [*Ghan et al.*, 2001].

Table 4: Aerosol composition parameters for ammonium sulfate and sea salt		
Parameter	*Ammonium Sulfate Value*	*Sea Salt Value*
Chemical Formula	$(NH_4)_2SO_4$	NaCl
Number of ions of dissociation, ν	3	2
Osmotic coefficient, φ	0.7	1.0
Solubility, ϵ	1.0	0.865*
Molecular weight, M_a	132	59
Density, ρ_a (g cm^{-3})	1.769	2.17*
Molecular weight of water, M_w **	18.016	18.016
Density of water, ρ_w (g cm^{-3}) **	1.0	1.0
Hygroscopicity parameter, B *** $\left(B = \frac{\nu\varphi\epsilon M_w \rho_a}{M_a \rho_w}\right)$	0.507	1.15

*: These values differ from [*Ghan et al.*, 2001] but still provide an accurate value for *B*.
**: These values are hard-coded into the parameterization routine.
***: *B* is calculated within the parameterization code rather than being passed as an argument; manually calculated here for display in the table.

Note that PCASP size bins between about 0.1 μm and 1 μm are affected by Mie scattering, and are only accurate assuming an index of refraction of 1.588 [*Liu and Daum*, 2000] (see section 2.2). This size range would include particles from the accumulation and coarse modes. Sea salt has an index of refraction of 1.544 [*Seinfeld and Pandis*, 2006], close to the calibration value, so errors from this effect would not be expected to be large for the coarse mode. Ammonium sulfate, however, has a somewhat lower index of refraction, 1.521 [*Weast*, 1987], so errors for the accumulation mode might be more significant. We tested the sensitivity to this error by increasing the median diameter for the accumulation mode; see Section 5.4.

4.3 Updraft Velocities

The ARG parameterization considers a Gaussian spectrum of in-cloud updraft velocities, requiring the mean $\overline{w}$ and standard deviation σ_w velocities to be specified. We specify $\overline{w}$ and σ_w based on the data taken by the aircraft during cloud penetrations. It is important to have a consistent definition for cloud penetrations which is used for both the calculations of mean and standard deviation updraft velocity, and the calculations of average cloud droplet concentration from FSSP and CDP, which are the observations to which the model results are compared. We use a CDP-derived liquid water content of .25 g m^{-3} as the criterion for cloud penetrations[11]. This is the LWC criterion used by two studies of cloud microphysics from the RICO campaign [*Colón-Robles et al.*, 2006; *Hudson and Mishra*, 2007][12].

Convection was found to be strongest in Leg 3 for the high wind case, and Leg 4 for the low wind case (see Figure 3) [*Smith et al.*, 2012]. Accordingly, updraft velocity data are taken from cloud penetrations in Leg 3 for the high wind flights, and Leg 4 for the low wind flights. These legs were flown multiple times in a single flight; data from cloud penetrations from all instances of the leg in question for the flight were used to calculate $\overline{w}$ and σ_w.

The updraft velocity measurement had a dependence on the angle of attack of the aircraft, which changed over the course of the flight as fuel was depleted. While a reanalyzed version of the data (used in this study) attempted to correct for this, the uncertainty in the $\overline{w}$ measurement is still fairly high, on the order of 0.5 m/s. (We have more confidence in σ_w, which was not affected as strongly by this problem.) Tests of the sensitivity of the model results to variations in $\overline{w}$ on the order of the level of uncertainty are described in Section 5.3.

4.4 Other Assumptions

The temperature of air at cloud base is assumed to be 300 K, or 26.8 °C, but from Table 2, temperatures at Leg 1L were actually between 23.4 and 24.8 °C; since about 400-500 m of lifting above Leg 1L would typically be required to reach cloud base [*Smith et al.*, 2012], the temperature at cloud base would be closer to about 20 °C, or 293 K, based on the dry adiabatic lapse rate of 9.8 °C/km. However, the cloud droplet activation process is only weakly sensitive

[11] FSSP-derived liquid water content was not used for this purpose because there were some discontinuities in the data record for LWC for that instrument, but not for CDP

[12] These two studies also required that "in-cloud" measurements have an updraft velocity > 0.5 m/s, but to filter data by updraft velocity would interfere with the calculation of $\overline{w}$ and σ_w.

to the temperature [*Ghan et al.*, 2011], which only affects the constants A, G, α, and γ used in the parameterization (see Section 3.3) [*Abdul-Razzak et al.*, 1998]. See Section 5.2 for a test of sensitivity to changes in temperature on the order of 7 K.

The droplet activation process is also weakly sensitive to pressure [*Ghan et al.*, 2011], which is also only used in the ARG parameterization to determine constants [*Abdul-Razzak et al.*, 1998]. Pressure can be calculated from temperature and air density, both of which are user-specified in the parameterization, using the equation of state, $p = \rho RT$. Air density is assumed for all model runs here to be 0.001275 g cm^{-3}.

5. Model Experiments: High Wind Case

The DOMEX flights that represent the high wind case are RF12, RF13, RF16, and RF17 (see Section 2). The modeling experiments for the high wind regime consist of a "standard run", which is a run of the ARG model based on our initial best-guess assumptions described in Section 4, and a series of sensitivity tests which involve changing various assumptions from the standard run, one at a time.

Section 5.1 describes the standard run. Sections 5.2 through 5.7 describe the results of the various sensitivity tests, and Section 5.8 is a discussion of the sensitivity tests taken together.

Observed cloud droplet concentrations from the CDP and FSSP probes from cloud penetrations in Leg 3 are included for comparison with the cloud droplet concentration predicted by the model.

5.1 Standard Run

See section 4 for an explanation of the "standard run" assumptions. These assumptions are summarized in the first part of Table 5. The second part of Table 5 shows the actual values obtained, for each of the four flights, for N_t, a_m, and σ for the four modes and for $\overline{w}$ and σ_w (see Section 4.1 for how the lognormal fit parameters were calculated, and Section 4.3 for how the updraft velocity parameters were derived). The third part of Table 5 shows the model results: the maximum supersaturation reached; the activation fraction for each mode; the droplet concentration for each mode (which is the activation fraction multiplied by that mode's N_t); and the total droplet concentration. The fourth part of Table 5 shows the observed droplet concentrations from the FSSP and CDP instruments. The observed droplet concentrations are averaged over the cloud penetrations in Leg 3, using the same LWC criterion for cloud penetrations used to calculate the mean and standard deviation updraft velocities. Figure 6 is a bar graph illustrating the last few lines of Table 5, comparing the modeled and observed droplet concentrations.

Table 5: “Standard run” of ARG model for flights RF12, RF13, RF16, and RF17 (high wind cases)

Assumptions common to all flights					
Mode composition:	Aitken mode	Ammonium sulfate (B = 0.507)			
	accumulation mode	Ammonium sulfate (B = 0.507)			
	coarse mode	Sea salt (NaCl) (B = 1.15)			
	giant mode	Sea salt (NaCl) (B = 1.15)			
Source air for aerosols		Average of Legs 1L and 1H			
Leg for cloud penetrations		Leg 3			
LWC criterion for cloud penetrations		0.25 g m^{-3}			
Cloud base temperature, T		300 K			
Cloud base air density, ρ_{air}		0.001275 g cm^{-3}			
Aitken mode median diameter, $a_{m,A}$ (μm)		0.0400			
Aitken mode geometric standard deviation, σ_A		1.5900			
Parameters obtained for specific flights					
Flight		RF12	RF13	RF16	RF17
Aitken mode number concentration, $N_{t,A}$ (cm^{-3})		309.1659	188.7157	194.2078	242.1256
accumulation mode:	med. diam., $a_{m,ac}$ (μm)	0.16748	0.17326	0.17391	0.16956
	geom. st. dev., σ_{ac}	1.3346	1.3238	1.3230	1.3175
	# conc., $N_{t,ac}$ (cm^{-3})	63.0903	73.6958	44.1049	71.0363
coarse mode:	med. diam., $a_{m,c}$ (μm)	0.69727	0.69025	0.69237	0.69875
	geom. st. dev., σ_c	1.3653	1.3472	1.2210	1.2703
	# conc., $N_{t,c}$ (cm^{-3})	2.1259	2.0310	0.80399	1.3025
giant mode:	med. diam., $a_{m,g}$ (μm)	1.7398	1.6900	1.4996	1.6917
	geom. st. dev., σ_g	1.3333	1.2822	1.2684	1.2801
	# conc., $N_{t,g}$ (cm^{-3})	0.12616	0.13346	0.060162	0.10349
Mean in-cloud updraft velocity, $\overline{w}$ (m/s)		1.6260	1.1317	0.97668	0.8012
St. dev. in-cloud updraft velocity, σ_w (m/s)		2.2442	1.8845	1.3330	1.9819
Model results					
Maximum supersaturation, S_{max}:		0.013419	0.012376	0.016049	0.012074
Activation fraction:	Aitken mode	0.315928	0.266017	0.279035	0.233011
	accumulation mode	0.755475	0.715026	0.758395	0.646751
	coarse mode	0.764728	0.72543	0.767351	0.657061
	giant mode	0.764830	0.725565	0.767428	0.657165
Max. theoretical activation fraction		0.765631	0.725923	0.768127	0.656989
Droplet concentration: (cm^{-3})	Aitken mode	97.67424	50.20153	54.19071	56.41790
	accumulation mode	47.66315	52.69443	33.44892	45.94278
	coarse mode	1.625736	1.473347	0.616943	0.855822
	giant mode	9.65E-02	9.68E-02	4.62E-02	6.80E-02
	total	**147.0596**	**104.4661**	**88.30274**	**103.2845**
Droplet observations					
Observed droplet conc.: CDP (cm^{-3})		**88.1252**	**90.6758**	**64.6817**	**74.9966**
Observed droplet conc.: FSSP (cm^{-3})		**90.3395**	**95.0190**	**71.9676**	**82.4292**

Color key: **(bold = plotted in Figure 6)**

Aitken mode	accumulation mode	coarse mode	giant mode	all modes

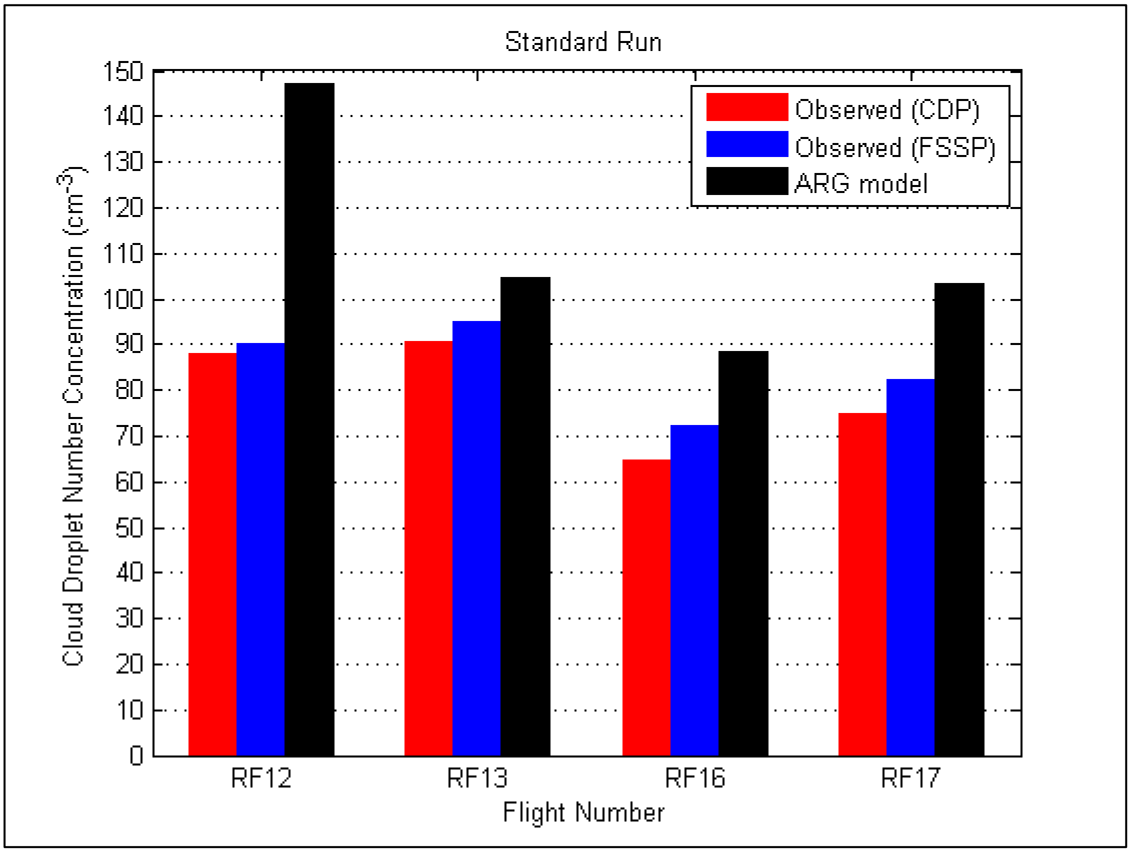

Figure 6. Observed and modeled total cloud droplet number concentrations, for all DOMEX high wind flights.

The modeled droplet concentration exceeds the observations for all four of the flights, to varying degrees. The modeled droplet concentration does not even always increase monotonically with the observed droplet concentration: RF12 has the highest modeled concentration, but a lower observed concentration than RF13.

The observed droplet concentrations from CDP and FSSP agree fairly well, so the discrepancy is probably due to the uncertainties in the model inputs and not in the observed droplet concentrations. One input that is potentially very uncertain is the mean updraft velocity. This measurement has uncertainty of about 0.5 m/s because the measured updraft velocity was dependent on the angle of inclination of the aircraft, which changed throughout the flight as fuel was depleted. The sensitivity test of the model results to 0.5 m/s changes in mean updraft velocity (see Section 5.3) is thus one of the most important in terms of interpreting the model results.

The breakdown of the results between the different modes is also informative. The activation fraction is, as would be expected, higher for the larger, sea salt modes than it is for the smaller, ammonium sulfate modes. The only reason that the activation fraction for the larger modes is not one is because the Gaussian updraft velocity distribution includes some negative values of *w*, for which the model assumes no particles are activated. See the “max. theoretical” activation fraction in Table 5, which is the area under the Gaussian PDF to the right of 0. (In some cases the modeled activation fraction may be slightly higher than the theoretical maximum; this is because of the model’s discrete treatment of the continuous PDF.)

Effectively all of the particles for the giant and coarse modes, and almost all of the particles for the accumulation mode, are activated whenever there is an updraft. The Aitken mode, by contrast, has a much smaller activation fraction, but it still accounts for about 1/2 to 2/3 of the droplets because a majority of the original aerosol particles are Aitken mode particles. All of the information for this mode effectively comes from one number: the CN concentration subtracted by the total PCASP concentration. Therefore, uncertainties in the assumptions about the Aitken mode are also very important. Note, in particular, that the amount by which RF12’s modeled droplet concentration exceeds that of RF13 can be accounted for entirely by the Aitken mode; the size distribution and composition in the Aitken mode are assumed to be the same for the two modes, but it could be the case that RF12’s Aitken mode particles are smaller and/or less hygroscopic, and we would have no way of knowing that from the CN observations. Section 5.4 describes a sensitivity test for the assumed position of the Aitken mode median diameter, $a_{m,A}$.

Testing the sensitivity of the model results to changes in various inputs and assumptions is useful for many reasons. In terms of model validation, looking at the direction of the change in the model results can help determine which changes in the assumptions would help bring the model into closer agreement with the observations. The magnitude of the change, meanwhile, can indicate the uncertainty of the model results in Figure 6. Also, the tests can provide insights into what factors are most important in determining the droplet activation fraction, and can help identify important variables to measure in a field campaign. Sections 5.2 through 5.7 include tests of the sensitivity of the model results to changes in:

- The cloud base temperature (Section 5.2)
- The mean updraft velocity (Section 5.3)
- The Aitken mode median diameter (Section 5.4)
- The accumulation mode median diameter (Section 5.5)
- The leg(s) used to calculate the aerosol lognormal parameters (Section 5.6)
- The LWC criterion for cloud penetrations, for both updraft velocity and measured droplet concentrations (Section 5.7)

5.2 Sensitivity Test: Cloud Base Temperature

To investigate the possible error from using 300 K as the cloud base temperature when 293 K might have been a better estimate (see Section 4.3), we ran the model with all of the standard run assumptions but with 293 K used as the cloud base temperature instead. The results, including modeled droplet concentrations for 300 K (the standard run) and 293 K, are summarized in Figure 7 and Table 6. See Table B1 in Appendix B for a more complete table analogous to Table 5 for the 293 K case.

The lower temperature leads to slightly higher modeled droplet concentrations, putting the model less in agreement with the observations. This difference is of a similar magnitude to the difference between the observed droplet concentrations, so it is not too significant, and running the other sensitivity tests at 300 K rather than 293 K should not invalidate the results. During DOMEX, the temperature at Leg 1L, and probably the cloud base temperature, varied by much less than 7 K (see Table 2), so cloud base temperature does not appear to be a major controlling factor for the activation fraction. However, the effect of temperature is not totally negligible, and this test would suggest that it is important to be able to estimate cloud base temperature to within a few K in order to accurately predict droplet activation.

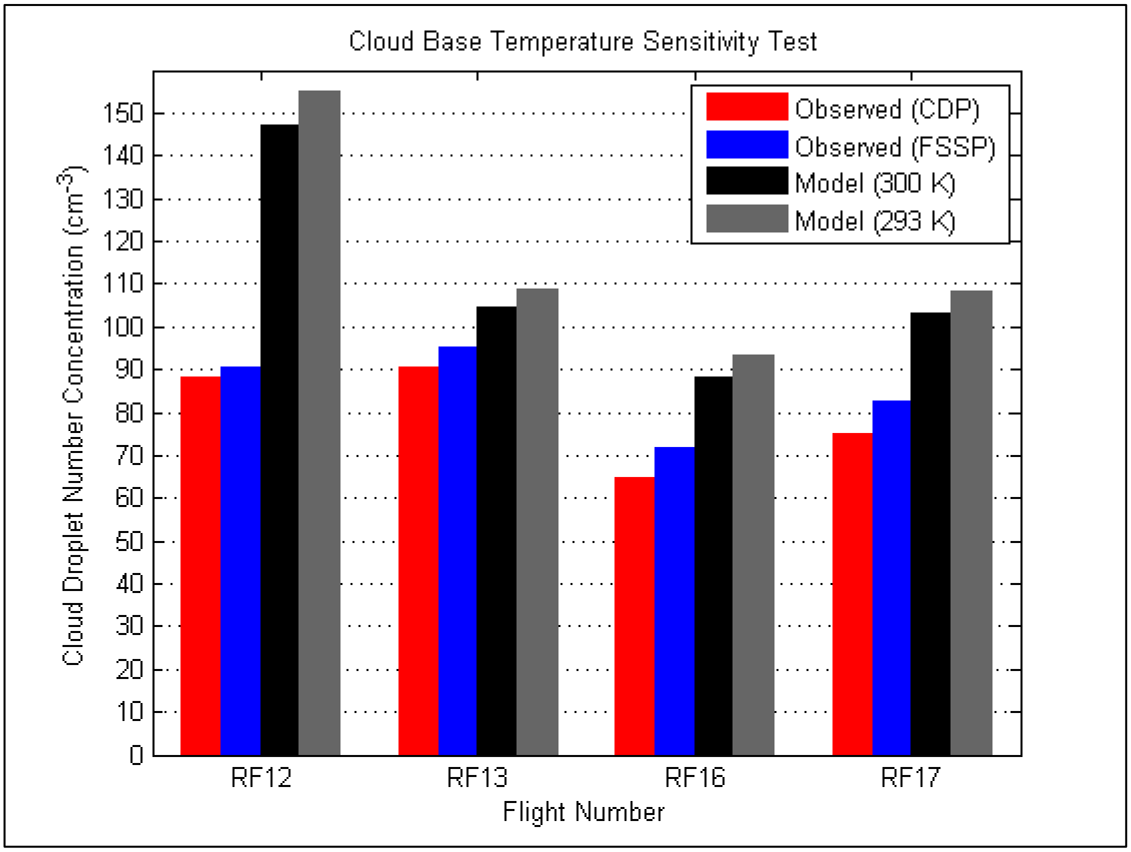

Figure 7. Sensitivity tests varying the cloud base temperature. Observed and modeled total cloud droplet number concentrations, for all DOMEX high wind flights, for 300 K (standard assumption) and 293 K.

Table 6: Sensitivity test of results of ARG model to 7 K change in cloud base temperature (high wind flights)				
Droplet concentrations (cm^{-3}):	RF12	RF13	RF16	RF17
Model results: 300 K (standard run)	147.0596	104.4661	88.3027	103.2845
Model results: 293 K	155.0636	108.9946	93.2969	108.4728
Observed droplet conc.: CDP	88.1252	90.6758	64.6817	74.9966
Observed droplet conc.: FSSP	90.3395	95.0190	71.9676	82.4292

5.3 Sensitivity Test: Mean Updraft Velocity

The mean updraft velocity measurement is very uncertain, on the order of maybe ± 0.5 m/s (see Section 5.1). The standard deviation is less uncertain because the angle of attack issue would, on the short time scale of the Leg 3 overpasses, have had much less of a significant impact on the variation about the mean value than on the mean value itself. In this test we ran the model with all of the standard run assumptions, but with 0.5 m/s added to $\overline{w}$, and again with 0.5 m/s subtracted from $\overline{w}$. The results of this test are summarized in Figure 8 and Table 7, and a more complete description of the two additional runs (including the values of $\overline{w}$ used for all of the flights in both cases) can be found in Tables B2 and B3 in Appendix B.

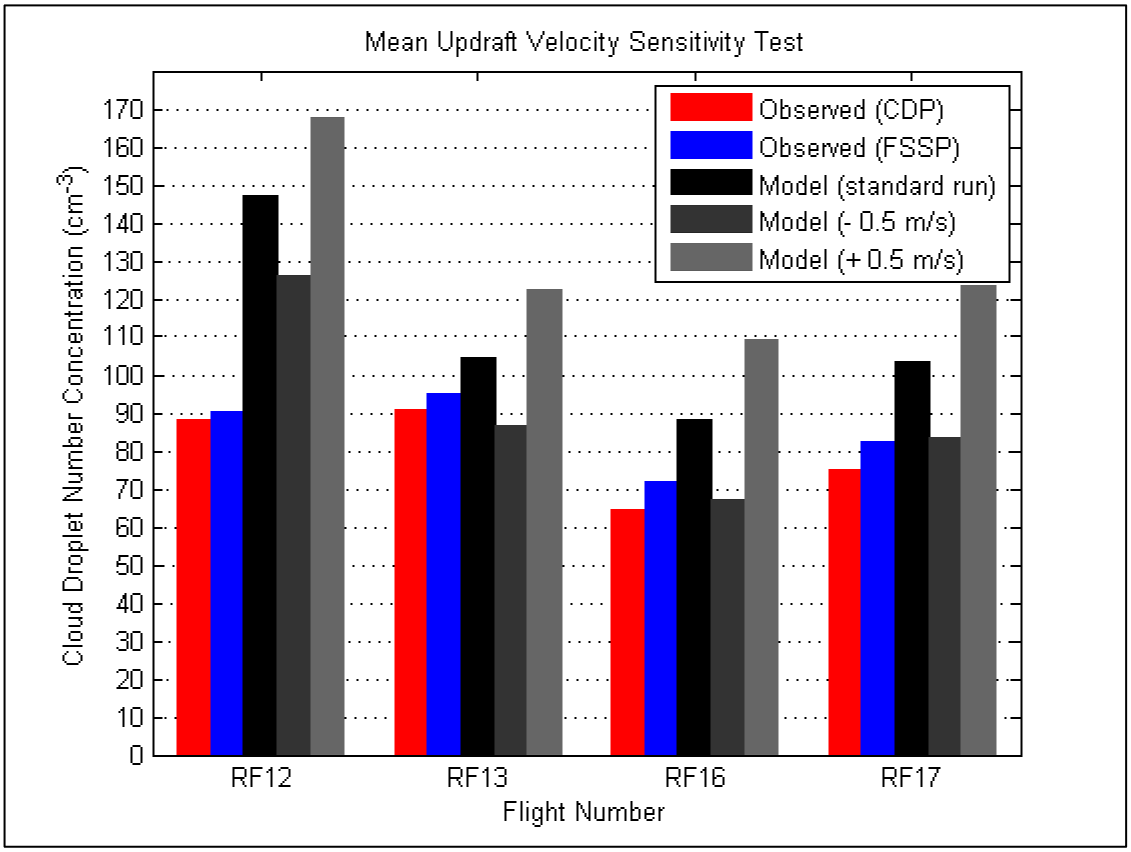

Figure 8. Sensitivity tests varying the mean updraft velocity. Observed and modeled total cloud droplet number concentrations, for all DOMEX high wind flights. Results for the standard run are shown in black; for the standard run with 0.5 m/s subtracted from $\overline{w}$ in dark gray; and for the standard run with 0.5 m/s added to $\overline{w}$ in light gray.

Table 7: Sensitivity test of results of ARG model to 0.5 m/s change in mean updraft velocity (high wind flights)				
Droplet concentrations (cm^{-3}):	RF12	RF13	RF16	RF17
Model results: standard run	147.0596	104.4661	88.3027	103.2845
Model results: standard run – 0.5 m/s	125.9706	86.4359	67.2482	83.6145
Model results: standard run + 0.5 m/s	167.8238	122.1567	108.9829	123.4572
Observed droplet conc.: CDP	88.1252	90.6758	64.6817	74.9966
Observed droplet conc.: FSSP	90.3395	95.0190	71.9676	82.4292

The model responds much more strongly to a 0.5 m/s change in the mean updraft velocity than to a 7 K change in temperature: the magnitude of the response in this test ranges from 18 to 22 cm^{-3} depending on the flight. This is enough to make the model results comparable to the observations in the "minus" case, for all of the flights except RF12. The 0.5 m/s value for the uncertainty, however, is somewhat arbitrary and it is conceivable that the error in the updraft velocity for RF12 could be much more than that. The strong sensitivity indicates that updraft velocity is a very important variable that must be measured accurately in order to feed models of droplet activation.

That higher updraft velocities lead to more droplets agrees with theory: a higher value of V leads to a higher value of dS/dt in equation (4), and hence a higher maximum supersaturation, activating smaller particles. Indeed, comparing the values of S_{max} for the same flights in Tables B2 and B3 shows that higher mean updraft velocity corresponds to higher supersaturation.

5.4 *Sensitivity Test: Aitken Mode Median Diameter*

Since the Aitken mode's median diameter was arbitrarily defined to be 0.040 μm, it is important to test the effects of changing that diameter. We ran the ARG model with the standard run assumptions except that $a_{m,A}$ was changed from 0.040 μm to 0.044 μm (the value from [*Seland et al.*, 2008]) and to 0.036 μm. To properly consider the effect of changing the value of $a_{m,A}$, all of the lognormal fit parameters for the four modes were recalculated according to the procedure described in Section 4 (although the effect on the coarse and giant modes would be negligible). The results of this test are summarized in Figure 9 and Table 8, and a more complete description of the two additional runs done for this test can be found in Tables B4 and B5 in Appendix B.

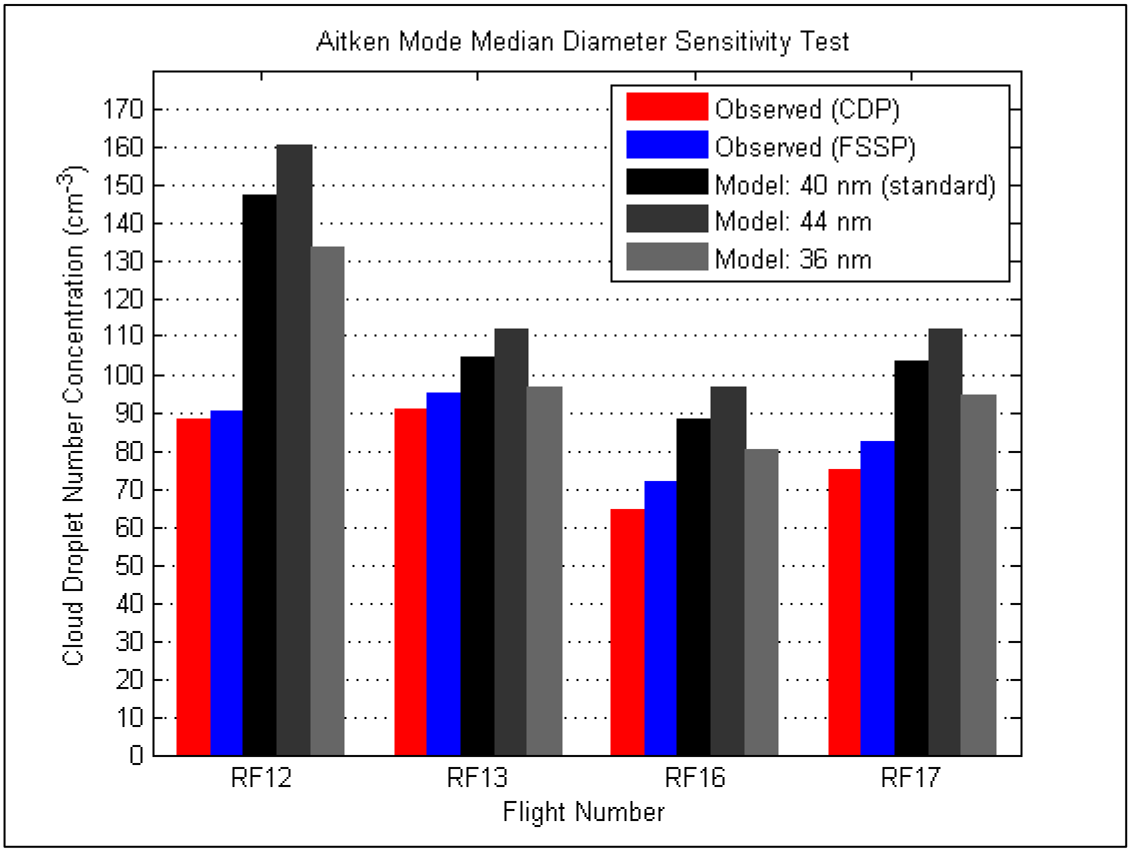

Figure 9. Sensitivity tests varying the Aitken mode median diameter. Observed and modeled total cloud droplet number concentrations, for all DOMEX high wind flights.

Table 8: Sensitivity test of results of ARG model to 4 nm change in Aitken mode median diameter (high wind flights)				
Droplet concentrations (cm^{-3}):	RF12	RF13	RF16	RF17
Model results: 40 nm (standard run)	147.0596	104.4661	88.3027	103.2845
Model results: 44 nm (standard + 4 nm)	160.5098	111.9080	96.6734	111.8355
Model results: 36 nm (standard – 4 nm)	133.1908	96.7830	80.0093	94.6752
Observed droplet conc.: CDP	88.1252	90.6758	64.6817	74.9966
Observed droplet conc.: FSSP	90.3395	95.0190	71.9676	82.4292

Changing the Aitken mode median diameter by 4 nm changes the modeled droplet number concentration by about 13 cm^{-3} for RF12 and about 8 cm^{-3} for the other three flights, a change 4 to 5 cm^{-3} greater than the changes from the temperature sensitivity test. These changes in the Aitken mode median diameter are not extreme, and 0.036 μm and 0.044 μm are plausible values for $a_{m,A}$ for DOMEX. The lack of information about the size distribution below 0.095 μm thus limits the ability to model droplet activation based on data inputs from DOMEX.

For campaigns such as RICO studying shallow oceanic clouds, updrafts are much weaker, so the small particles may not be as relevant in those situations. But in situations with strong updrafts, like orographic convection (as in this study) and deep convection, higher supersaturations are reached, activating the smaller particles. This suggests that future field campaigns interested in cloud microphysics in regimes with strong updrafts should devote resources to observations that resolve the size distribution for particles smaller than 0.1 μm.

Comparing the breakdowns of droplet activation by mode in Tables 5, B4 and B5 is informative. With increasing Aitken mode median diameter from 0.040 to 0.044 μm, the activation fractions of both the Aitken and accumulation modes increase. For both modes this is because the particles, on average, are larger, and larger particles have a lower critical supersaturation. The accumulation particles are larger on average because the Aitken mode subtraction from the accumulation mode's PCASP bins (from 0.095 to 0.491 μm; see section 4.1.1) affects the smallest bins more. The Aitken mode is responsible for most of the increase in the overall activation fraction, partly because the activation fraction for the accumulation mode is already close to the theoretical maximum in the standard run.

5.5 Sensitivity Test: Accumulation Mode Median Diameter

Due to Mie scattering, the particles between about 0.1 and 1 μm in diameter are larger than their apparent diameter measured by PCASP, if the index of refraction is less than 1.588 [*Liu and Daum*, 2000]. Ammonium sulfate has an index of refraction of 1.521 [*Weast*, 1987], so the accumulation mode particle diameters might be affected by this. The accumulation mode includes particles up to 0.491 μm in diameter. According to *Liu and Daum*, for a particle with apparent diameter 0.45 μm and an index of refraction of 1.5, the actual diameter is 0.51 μm (see pg. 952), an error of 0.06 μm. The error for an index of refraction greater than 1.5 should be less than 0.06 μm, and most of the particles in the accumulation mode have diameters smaller than 0.45 μm, for which the error caused by this effect is lower. So increasing the accumulation mode median diameter by 0.05 μm would be a conservative test that would encapsulate all of the possible error from the Mie scattering effect.

For this test, 0.05 μm is added to the accumulation mode median diameter from the standard run. No effect is considered on the other modes because this test assumes that there is the same number of particles in the accumulation mode, but that they are larger. The results are summarized in Figure 10 and Table 9, and a more complete summary of the additional run done for this test is given in Table B6 in Appendix B.

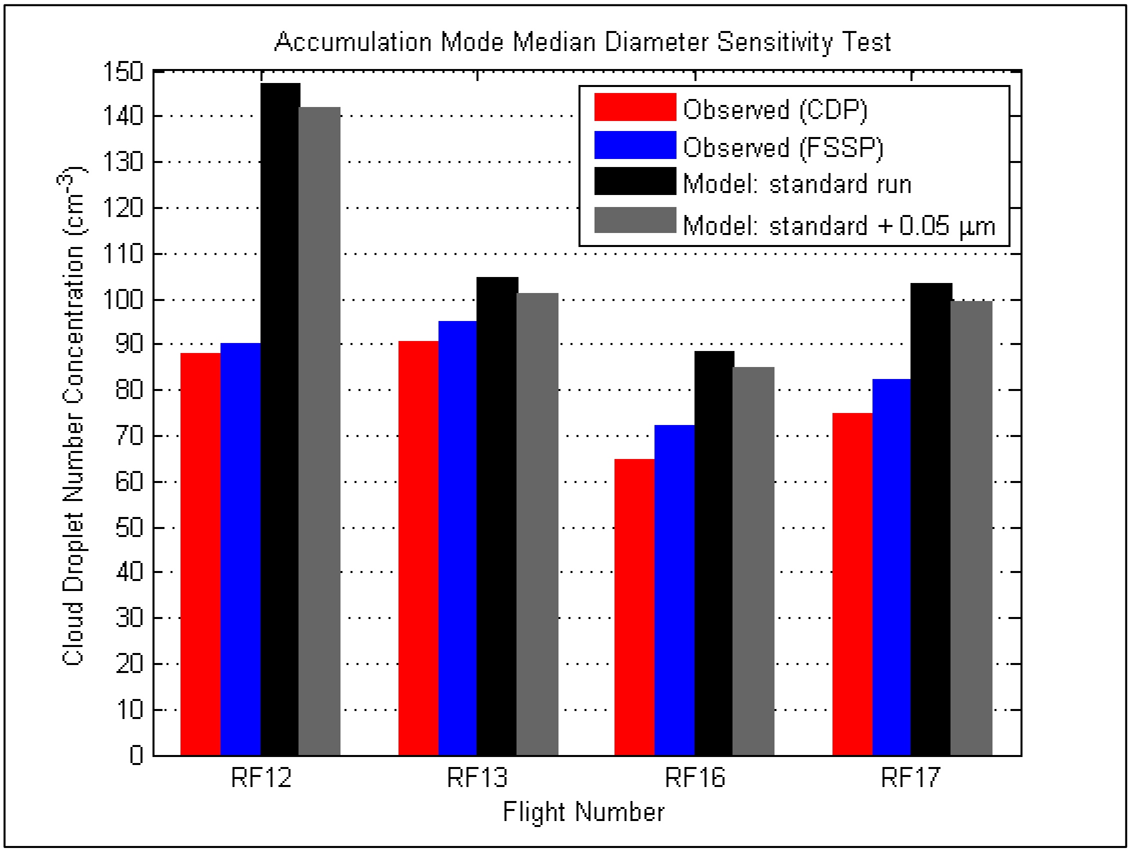

Figure 10. Sensitivity tests varying the accumulation mode median diameter. Observed and modeled total cloud droplet number concentrations, for all DOMEX high wind flights.

Table 9: Sensitivity test of results of ARG model to 50 nm change in accumulation mode median diameter (high wind flights)

Droplet concentrations (cm^{-3}):	RF12	RF13	RF16	RF17
Model results: standard run	147.0596	104.4661	88.3027	103.2845
Model results: standard + 50 nm	141.7811	100.9751	84.8298	99.3496
Observed droplet conc.: CDP	88.1252	90.6758	64.6817	74.9966
Observed droplet conc.: FSSP	90.3395	95.0190	71.9676	82.4292

The overall activation fraction and droplet concentration actually drop with the increase in the accumulation mode median diameter. Looking at Table B6 explains why: the activation fraction of the accumulation mode does increase slightly compared to the standard run, but the activation fraction of the Aitken mode decreases by more than enough to compensate (the effect on the larger two modes is negligible). A physical explanation of this is that more water vapor is taken up by the accumulation mode, leaving less available to activate the smallest particles in the Aitken mode. A mathematical explanation is that the critical supersaturation at median radius $S_{m,i}$ for the accumulation mode is larger in equation (9), so the maximum supersaturation S_{max} is lower, activating less particles in the Aitken mode. To confirm this, compare the values of S_{max} in Tables 5 and B6.

The magnitude of the change in the modeled droplet concentration for this sensitivity test is small, less than 6 cm^{-3}. Most of the particles in the Aitken mode probably have a real diameter that differs from the apparent diameter by much less than 0.05 μm, so it is likely that the real error from the Mie scattering effect is much less than that from this test. For the Mie scattering effect on the coarse mode, we would expect the error to be even smaller, because sea salt has a larger index of refraction than ammonium sulfate and because effectively all of the coarse mode particles were already being activated. We can conclude that the errors in the PCASP size bins caused by Mie scattering are not a significant source of error in our model runs, given our assumptions about the aerosol composition.

5.6 Sensitivity Test: Aerosol Source Air

For the standard run, the air for the clouds in the high wind cases was assumed to come from between 300 m and 1200 m, the altitudes of Legs 1L and 1H, respectively, and the leg-averaged CN and PCASP particle concentrations from those 2 legs were averaged together before the fitting of lognormal modes to the aerosol observations. This test examined the possible error from this assumption, by looking at the two legs individually. The results are summarized in Figure 11 and Table 10; Tables B7 and B8 in Appendix B give a more complete description of the model runs using Leg 1L only and Leg 1H only, respectively.

This test differs from the previous sensitivity tests in that the sensitivity of the model results varies dramatically by flight. The difference between the modeled droplet concentrations between the 1L and 1H cases varies from less than 3 cm^{-3} in for RF12, to almost 22 cm^{-3} for

RF17. The reason for this variation can be seen by comparing the Aitken and accumulation mode particle concentrations from Tables B7 and B8: the differences in these concentrations between Legs 1L and 1H are strongest for RF13 and RF17, and weakest for RF12. RF16 is an interesting case: unlike the other flights, it actually has a higher Aitken mode concentration at 1200 m than 300 m, but also has the strongest difference between the accumulation mode concentrations between the legs.

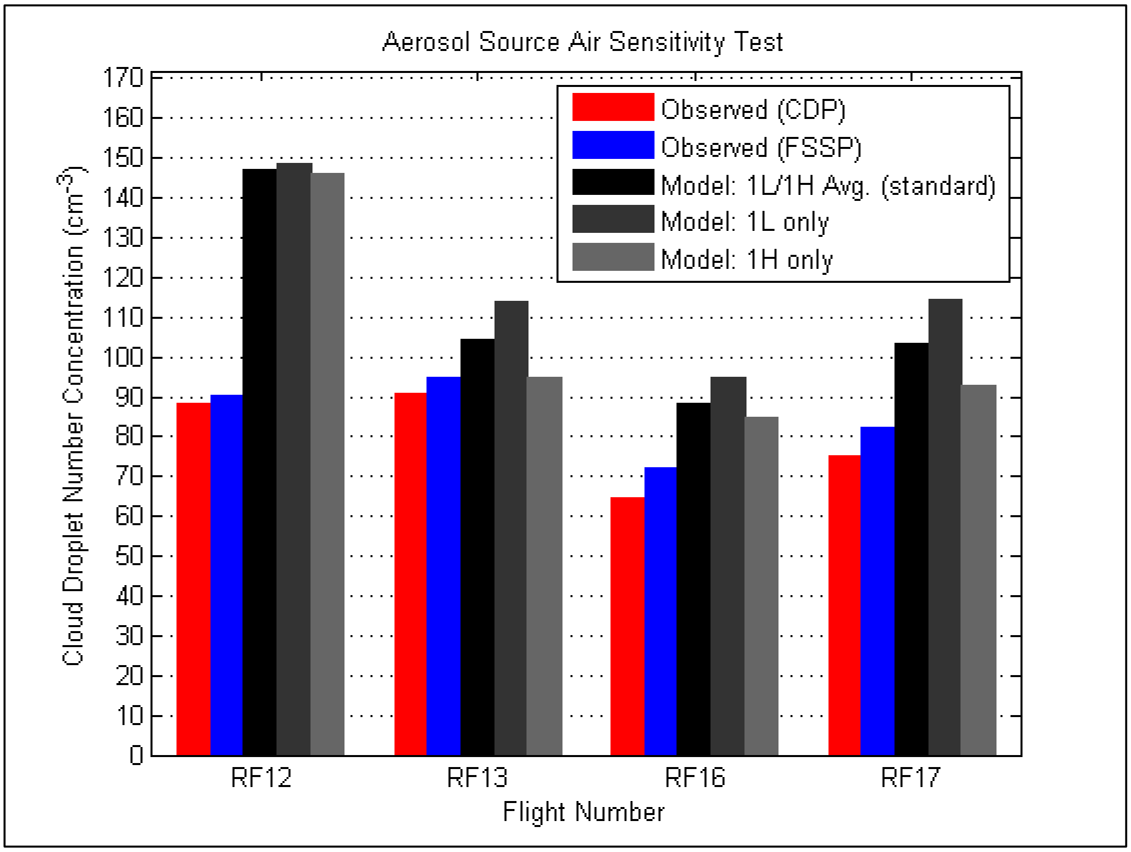

Figure 11. Sensitivity tests varying the source of input aerosol. Observed and modeled total cloud droplet number concentrations, for all DOMEX high wind flights.

Table 10: Sensitivity test of results of ARG model to upwind leg used for aerosol source air (high wind flights)				
Droplet concentrations (cm^{-3}):	RF12	RF13	RF16	RF17
Model results: 1L and 1H average (standard)	147.0596	104.4661	88.3027	103.2845
Model results: 1L only	148.5888	113.8592	95.0111	114.6163
Model results: 1H only	145.8849	94.9376	84.9299	92.8550
Observed droplet conc.: CDP	88.1252	90.6758	64.6817	74.9966
Observed droplet conc.: FSSP	90.3395	95.0190	71.9676	82.4292

This test would suggest that when there is a strong vertical gradient of particle concentration, knowing the location of the source air is important. On the other hand, since these are convective clouds, the size spectra between altitudes of 300 and 1200 m may in fact literally be averaged by turbulent vertical mixing, and the air in the clouds should not be thought of as coming from a thin layer at one specific altitude. It should also be noted that the individual clouds in the regime are not identical, and different cloud penetrations showed different droplet concentrations, and the droplet concentrations. Still, the results from using legs 1L and 1H separately provide a good idea of the range of possible outcomes due to the uncertainty in the location of the source air.

5.7 Sensitivity Test: Cloud Penetration LWC Criterion

Since the ARG model does not consider entrainment of dry air on the sides of the cloud, it seemed possible that the agreement between the model and observations could be improved by looking closer to the center of the clouds. This could be done by increasing the liquid water content criterion used to define cloud penetrations (.25 g m^{-3} in the standard run). This would increase the observed CDP and FSSP droplet concentrations, but it would also increase the mean updraft velocities fed to the model and hence the modeled droplet concentrations. This test was an experiment to see whether increasing the LWC criterion would bring the model and observations closer together, or push them farther apart. LWC criteria of .30, .40, and .50 g m^{-3} were tried. The results are summarized in Figure 12 and Table 11, and the three additional model runs are described in detail in Tables B9, B10, and B11 in Appendix B.

As shown in Table 11, the mean updraft velocity increases with increasing LWC criterion, indicating that this is a way of moving closer to the updraft cores at the center of the clouds. The observed droplet concentration did indeed go up, but due to the higher updraft velocity, the modeled droplet concentration increased by more than enough to compensate. Focusing on the cores of the clouds does not, as might be expected, make the model agree more with the observations. This effect emphasizes the large sensitivity of the model results to small changes in the mean updraft velocity.

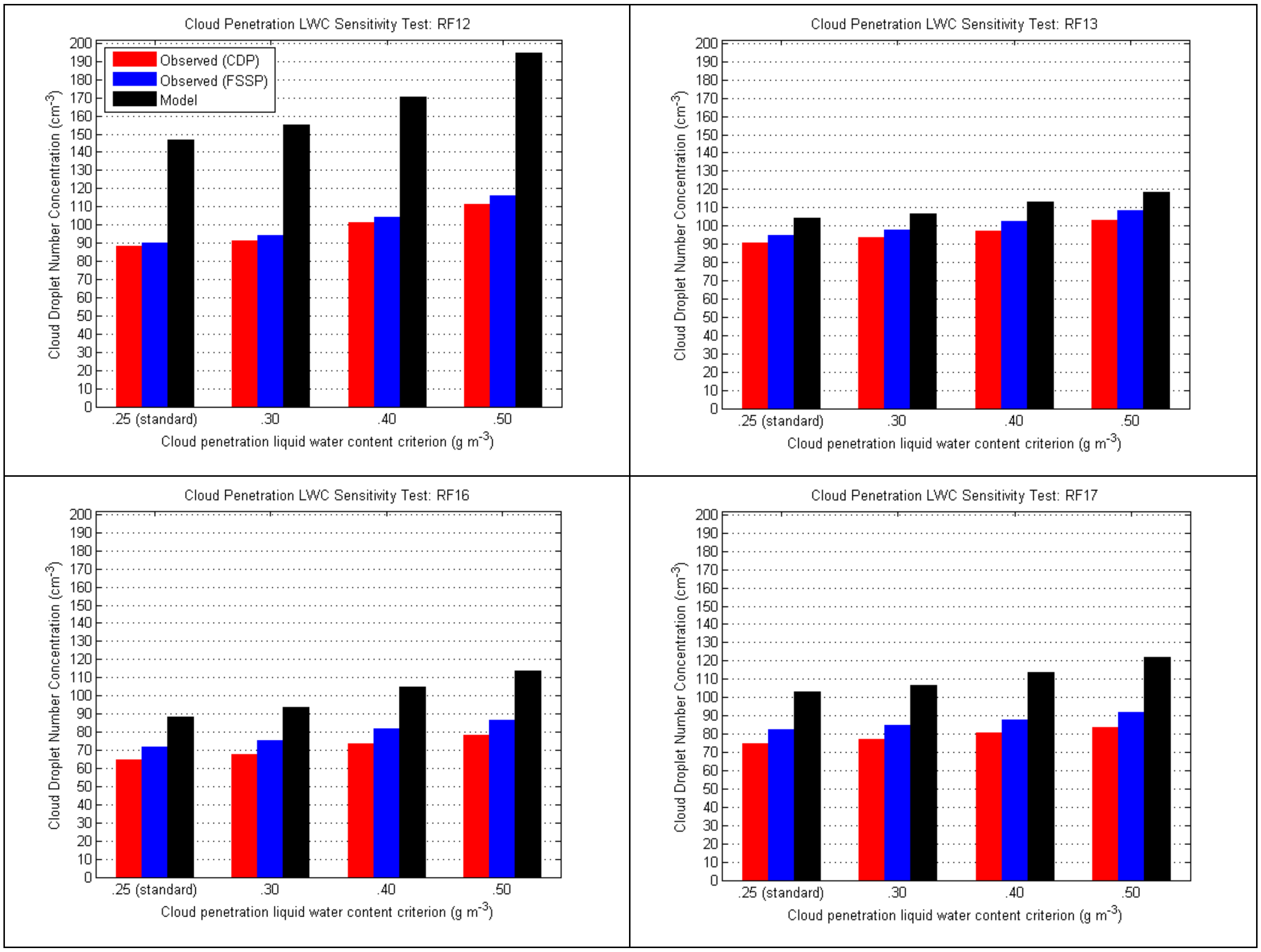

Figure 12. Sensitivity tests varying the liquid water content criterion for cloud penetrations. Unlike the other sensitivity tests, this time the observations change as well as the model results. Each of the four bar graphs represents a flight; within these graphs, the data are grouped by LWC criterion.

Table 11: Sensitivity test of observed droplet concentration, and results of ARG model, to LWC criterion used for cloud penetrations (high wind flights)				
LWC criterion (g cm^{-3})	0.25	0.3	0.4	0.5
RF12				
Mean updraft velocity (m/s)	1.626	1.8077	2.2147	2.815
CDP droplet conc. (cm^{-3})	88.1252	91.4388	101.1052	111.0791
FSSP droplet conc. (cm^{-3})	90.3395	94.0158	104.3182	116.1605
Model droplet conc. (cm^{-3})	147.05962	154.81122	170.64519	194.72745
RF13				
Mean updraft velocity (m/s)	1.1317	1.1864	1.3657	1.5203
CDP droplet conc. (cm^{-3})	90.6758	93.618	97.4155	103.0236
FSSP droplet conc. (cm^{-3})	95.019	97.9148	102.276	108.3799
Model droplet conc. (cm^{-3})	104.46614	106.38583	112.92631	118.61205
RF16				
Mean updraft velocity (m/s)	0.9769	1.1125	1.3851	1.6186
CDP droplet conc. (cm^{-3})	64.6817	67.5774	73.5488	78.496
FSSP droplet conc. (cm^{-3})	71.9676	75.4935	81.511	86.794
Model droplet conc. (cm^{-3})	88.302742	93.783752	104.80102	113.7624
RF17				
Mean updraft velocity (m/s)	0.8012	0.876	1.0535	1.2607
CDP droplet conc. (cm^{-3})	74.9966	77.1107	80.3381	83.6832
FSSP droplet conc. (cm^{-3})	82.4292	84.7854	87.496	91.5857
Model droplet conc. (cm^{-3})	103.28452	106.32658	113.45761	121.83633

5.8 Discussion of Sensitivity Tests

Based on the tests described above, there are several observations to be made about what controls the modeled droplet concentration. One is that the mean updraft velocity appears to be the variable to which the results are most sensitive: besides the large differences in the results for when the mean updraft velocities were directly changed (Section 5.3), the change in updraft velocity for the LWC criterion test was also enough to overcome the higher observed droplet concentration in the updraft cores (Section 5.7). The other major observation is that the Aitken mode is very important in determining the activation fraction: small changes in the Aitken mode median diameter had a large impact on the total activation fraction (Section 5.4), and small changes in the accumulation mode median diameter had the opposite than expected effect on the total activation fraction, because the change in the Aitken mode's activated droplets, due to changes in the amount of water vapor taken up by the accumulation mode, dominated the change in the accumulation mode's activated droplets (Section 5.5).

In terms of the agreement between the modeled and observed droplet concentrations, the wind speed sensitivity test alone was enough to make the model agree with the observations for RF13, RF16, and RF17. But for RF12, even if all of the reductions in the modeled droplet concentration from all of the tests were combined (assuming they could be added linearly), the model results would still overestimate the observations. It is an important question to resolve why RF12 is so different.

One possible explanation is that the dynamics are different for RF12. RF12 has the strongest updrafts in Leg 3 cloud penetrations, and the most similar aerosol concentrations between Legs 1L and 1H, indicating more vertical mixing upwind. Differences in the flow patterns compared to the other flights could affect, for example, the location of the source air for the clouds, but note from Section 5.6 that the sensitivity to the source air is very small for RF12. Also, if orographic convection and precipitation started further east for RF12 than for the other flights, which is plausible given RF12's higher updraft velocity, it may be possible that RF12 had a lower measured droplet concentration in Leg 3 because there was more loss of droplets due to droplet collision and coalescence and precipitation further east. Another consideration is that pre-existing cloud droplets from the upwind air could have grown more upon orographic uplift, taking water vapor away that otherwise would have gone toward activating the smaller droplets. Note that the model assumes initially cloud-free air, and the aerosol size distributions were taken from air with LWC < 0.003 g m^{-3}, but the actual clouds over the island often form around pre-existing clouds. These last two considerations, however, would affect all of the high wind flights, not just RF12, and upwind clouds and precipitation were observed for all four high-wind flights. The question of whether precipitation east of Leg 3 and pre-existing clouds in the source air could have caused a discrepancy between the model and observations, and in particular, whether it could have affected RF12 more than the other flights, needs to be investigated further. Looking at the cloud droplet size distributions from the CDP and FSSP probes may help answer this question.

Another explanation for how RF12 could have differed from the other high wind flights is that the composition or size distribution in the Aitken mode was different. RF12 has by far the strongest Aitken mode concentration, which may not necessarily imply a larger activation fraction if RF12's Aitken mode particles were smaller, or less hygroscopic, than those in the other flights. Possible sources of small or less hygroscopic particles for the RF12 Aitken mode include organic aerosols from the ocean, and black carbon from ship tracks, both of which are not very hygroscopic; while there were no obvious ship track signatures in the time series of the RF12 CN concentration for Leg 1L, there could have been well-mixed ship emissions from, for example, the night before the flight. But without observational data on the size distribution and composition of the Aitken mode particles, we can only speculate on this question. This underscores the importance of taking such data during similar campaigns in the future.

6. Model Experiments: Low Wind Case

For the low wind cases, the aerosols in the source air for the clouds are thought to be largely island-derived, and there are no data from DOMEX about the composition of island-derived aerosols. To see how well our assumptions about the aerosol composition for the high wind flights hold up when applied to the low wind flights (RF07 and RF08), we ran the model with the aerosol size distribution taken from out-of-cloud air (LWC < 0.003 g m^{-3}) in Leg 4 (the closest observations to the aerosols' island source), and with updraft velocities and observed droplet concentrations taken from in-cloud air (LWC > 0.25 g m^{-3}) also in Leg 4. To eliminate the oversea portion at the northern and southern ends of Leg 4, the first and last two minutes of the leg (as defined by the mission scientist's flight notes) were excluded. The assumptions, lognormal parameters, observations, and model results from this experiment are summarized in Table 12; Figure 13 compares the model results and observations graphically.

Table 12: Run of ARG model for flights RF07 and RF08 (low wind cases)			
Assumptions common to both flights			
Mode composition:	Aitken mode	Ammonium sulfate (B = 0.507)	
	accumulation mode	Ammonium sulfate (B = 0.507)	
	coarse mode	Sea salt (NaCl) (B = 1.15)	
	giant mode	Sea salt (NaCl) (B = 1.15)	
Source air for aerosols		Detraining air in Leg 4	
Leg for cloud penetrations		Leg 4	
LWC criterion for cloud penetrations		0.25 g m^{-3}	
Cloud base temperature, T		300 K	
Cloud base air density, ρ_{air}		0.001275 g cm^{-3}	
Aitken mode median diameter, $a_{m,A}$ (µm)		0.0400	
Aitken mode geometric standard deviation, σ_A		1.5900	
Parameters obtained for specific flights			
Flight		RF07	RF08
Aitken mode number concentration, $N_{t,A}$ (cm^{-3})		734.3243	977.2178
accumulation mode:	med. diam., $a_{m,ac}$ (µm)	0.16053	0.18313
	geom. st. dev., σ_{ac}	1.4100	1.3041
	# conc., $N_{t,ac}$ (cm^{-3})	256.8770	301.6442
coarse mode:	med. diam., $a_{m,c}$ (µm)	0.69987	0.69444
	geom. st. dev., σ_c	1.7003	1.4140
	# conc., $N_{t,c}$ (cm^{-3})	0.46125	0.43387
giant mode:	med. diam., $a_{m,g}$ (µm)	2.8682	1.7802
	geom. st. dev., σ_g	1.0292	1.3066
	# conc., $N_{t,g}$ (cm^{-3})	0.0016718	0.024331
Mean in-cloud updraft velocity, $\overline{w}$ (m/s)		1.6326	1.7459
St. dev. in-cloud updraft velocity, σ_w (m/s)		2.0999	1.6996
Model results			
Maximum supersaturation, S_{max}		0.009106	0.007440
Activation fraction:	Aitken mode	0.197115	0.166171
	accumulation mode	0.757969	0.831018
	coarse mode	0.779972	0.845758
	giant mode	0.780695	0.846341
Max. theoretical activation fraction		0.781558	0.847847
Droplet concentration: (cm^{-3})	Aitken mode	144.7462	162.3848
	accumulation mode	194.7049	250.6717
	coarse mode	0.359762	0.366949
	giant mode	1.31E-03	2.06E-02
	Total	**339.8122**	**413.4440**
Droplet observations			
Observed droplet conc.: CDP (cm^{-3})		**313.3660**	**393.2740**
Observed droplet conc.: FSSP (cm^{-3})		**331.0513**	**405.9965**

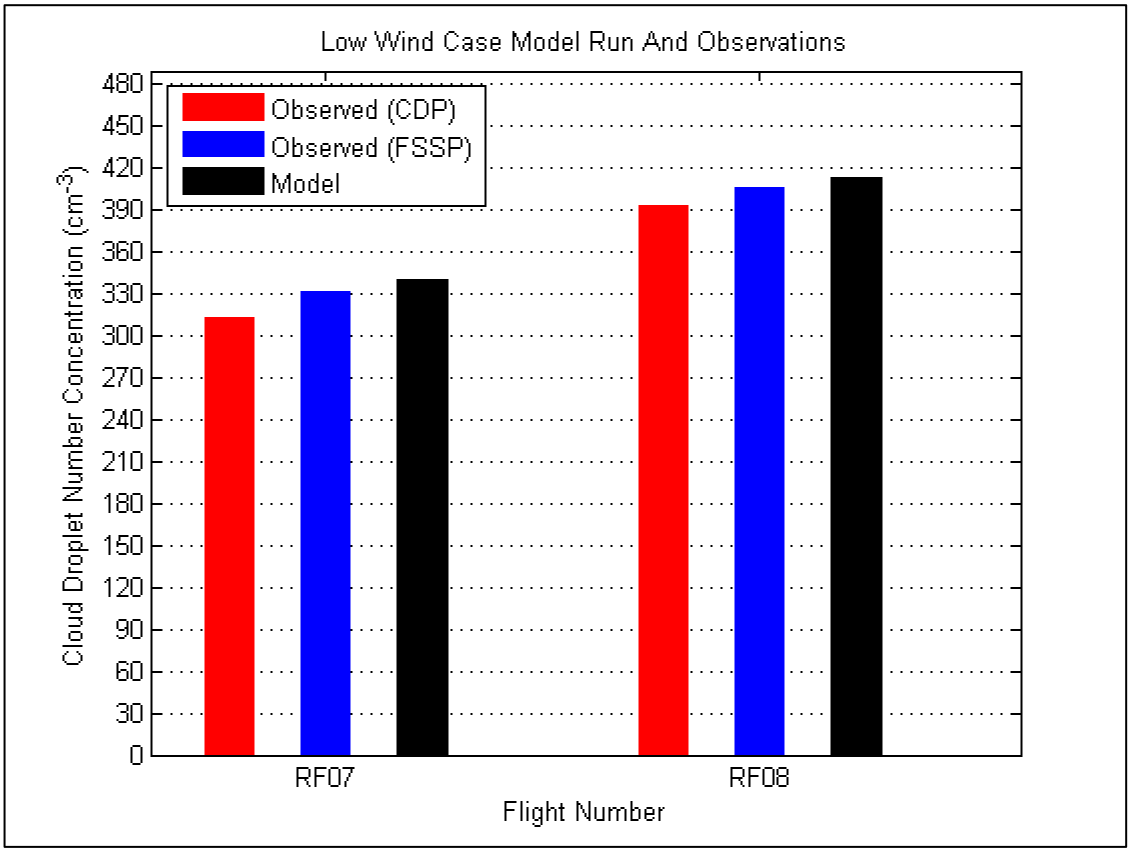

Figure 13. Model run and observations for the DOMEX low wind flights.

The model predicts the observations surprisingly well in this case, given the lack of information about the composition. For both RF07 and RF08, the modeled droplet concentration differs from the FSSP value by less than the FSSP differs from the CDP. This is better agreement than for the high wind flights under the "standard run" assumptions, and one of the high wind flights, RF12, does not have this kind of agreement with the observations under any of the sensitivity tests either.

This agreement may simply be a coincidence, and further work, including sensitivity tests similar to those for the high wind cases, is necessary to test how robust the model results are when the assumptions used are changed. Still, it suggests that it may be possible to model droplet activation in thermally driven, tropical, orographic regimes using 2 ammonium sulfate modes and two sea salt modes. Note from Table 12 that the Aitken and accumulation modes have a much higher particle concentration here than for the high wind flights; that the coarse mode is much less prevalent; and that the giant mode is virtually absent, especially for RF07. This suggests that even using only the two sulfate modes may be a good approximation. This would be an interesting sensitivity test to try in the future.

Since Dominica is a volcanic island, island-derived sulfate particles would be expected, and the island is known to smell of sulfur. Even if some of the particles in the Aitken mode were not sulfates (e.g. organic or anthropogenic aerosols), the ammonium sulfate assumption for the Aitken mode would still work well if the non-sulfate aerosols in the Aitken mode were too small to have been activated, had they been sulfate. The maximum supersaturation for this experiment is lower than for any of the high wind case runs (see Table 12), likely because a higher total number of droplets increased the sink term of supersaturation in equation (4); this resulted in a lower activation fraction, implying only larger particles activated, for the Aitken mode and may well have prevented small, non-sulfate particles from affecting the results.

Thus, there is reason to believe that using entirely ammonium sulfate for the Aitken and accumulation mode aerosols may be sufficient to predict droplet activation in regimes like the DOMEX low wind case, and that detailed knowledge of the aerosol composition may not be necessary. Sensitivity tests to the inclusion of additional modes containing other types of aerosol would be needed to confirm this.

7. Conclusions and Future Work

For the high wind flights, using the ARG parameterization to attempt to predict the observed droplet concentration, based on the upwind aerosol data and in-cloud updraft velocity, resulted in model results that overestimated the observations for all four flights, for the "standard run" assumptions. Errors from 0.5 m/s uncertainty in mean updraft velocity are enough to reconcile these differences for all of the high wind flights except RF12. For RF12, the combined errors from all sensitivity tests still are not enough to make the model agree with the observations. Possible reasons for the different behavior of RF12 include dynamical differences, and differences in the size distribution and/or hygroscopicity of the Aitken mode particles, between RF12 and the other high wind days. Research in the near future, involving examining the droplet size distributions from CDP and FSSP and performing sensitivity tests to changes in the Aitken mode composition, will attempt to determine which of these explanations are most likely correct.

Sensitivity tests for the high wind flights showed that the model results are very sensitive to changes in the mean updraft velocity and the Aitken mode's median diameter. The sensitivity to the choice of cloud source air between Leg 1L, 1H, or an average of both depends on the vertical gradient of aerosol concentration, which was strongest for RF13 and RF17 and smallest for RF12. Focusing on the centers of the clouds by increasing the LWC criterion for cloud penetrations increases the discrepancy between modeling and observations, because the increase in the updraft velocity overcompensates for the increase in the observed droplet concentrations. The sensitivity to cloud base temperature was less important, and the sensitivity to changes in the accumulation mode associated with the Mie scattering effect on the PCASP size bins were practically nonexistent, indicating that this effect is not a concern given our assumptions about the aerosol composition.

In terms of measurement considerations, for the high wind regime, the sensitivity tests suggest that accurate measurements of wind speed, and of the size distribution for particles smaller than 0.1 μm, are extremely important. The cloud base temperature is less important but should be estimated to within several K. The importance of knowing the aerosol composition, beyond assuming ammonium sulfate for the smaller two modes and sea salt for the larger two modes, remains unresolved; future sensitivity tests involving adding other aerosol species, such as an organic mode, will attempt to answer this question.

For the low wind flights, with the same assumptions about the aerosol composition, the model results matched the observations better than for the high wind flights. Future sensitivity tests similar to those performed for the high wind case will attempt to establish the possible error around the model results for this case, to see whether the agreement between the model results and observations is simply a coincidence or is more robust. If this agreement can be trusted, it would suggest that assuming that all of the Aitken and accumulation mode particles are ammonium sulfate may be sufficient to predict the droplet activation fraction in this regime, since the model only activates the larger particles in the Aitken mode which are more likely to be sulfate. Sensitivity tests to addition of non-sulfate modes (such as organic aerosol) will be needed to confirm this hypothesis.

Having established a set of assumptions and sensitivity tests for running the ARG parameterization based on DOMEX aerosol data, it would be interesting to apply the same assumptions and tests to other models. Doing similar tests with other droplet activation parameterizations could make the conclusions about what is important to measure in order to predict the activation fraction more robust, and could be used to investigate the effects of specific aspects of the ARG parameterization, such as neglecting kinetic effects, by looking at the behavior of a model which differed in those aspects. Perhaps the most intriguing potential avenue would involve applying the same assumptions and sensitivity tests used in this study to a cloud-resolving model, such as WRF, using the ARG parameterization as the embedded droplet activation scheme. That would allow for modeling studies, constrained by the aerosol data from DOMEX, that would go beyond the droplet activation stage and through the entire life cycle of clouds.

Acknowledgements

Jeffrey French of the University of Wyoming was instrumental in helping me interpret the observations, particularly the CDP and FSSP droplet concentrations. Yong Cai, also of the University of Wyoming, helped bring my attention to the Mie scattering issue for the PCASP size distributions and pointed me in the right direction to address it.

The scientists in the DOMEX research group provided useful feedback and suggestions on my project. Justin Minder suggested looking in the updraft cores to avoid the effects of entrainment, which led to the LWC criterion sensitivity test.

The Yale Climate and Energy Congress provided me with a travel grant to attend the 2011 American Geophysical Union Fall Meeting, where I presented a poster on my progress on this project and received much useful feedback.

References Cited

Abdul-Razzak, H., and S. J. Ghan (2000), A parameterization of aerosol activation 2. Multiple aerosol types, *J. Geophys. Res.*, *105*(D5), 6837-6844.

Abdul-Razzak, H., and S. J. Ghan (2002), A parameterization of aerosol activation 3. Sectional representation, *J. Geophys. Res.*, *107*(D3), 4026.

Abdul-Razzak, H., S. J. Ghan, and C. Rivera-Carpio (1998), A parameterization of aerosol activation 1. Single aerosol type, *J. Geophys. Res.*, *103*(D6), 6123-6131.

Colón-Robles, M., R. M. Rauber, and J. B. Jensen (2006), Influence of low-level wind speed on droplet spectra near cloud base in trade wind cumulus, *Geophys. Res. Lett.*, *33*(20), L20814.

Forster, P., et al. (2007), Changes in Atmospheric Constituents and in Radiative Forcing, in *Climate Change 2007: The Physical Science Basis. Contribution of Working Group I to the Fourth Assessment Report of the Intergovernmental Panel on Climate Change*, edited by S. D. Solomon, M. Qin, Z. Manning, M. Chen, K. B. Marquis, M. Averyt, M. Tignor and H. L. Miller, pp. 129-234, Cambridge University Press, Cambridge, United Kingdom and New York, NY, USA.

Ghan, S. J., N. Laulainen, R. Easter, R. Wagener, S. Nemesure, E. Chapman, Y. Zhang, and R. Leung (2001), Evaluation of aerosol direct radiative forcing in MIRAGE, *J. Geophys. Res.*, *106*(D6), 5295-5316.

Ghan, S. J., H. Abdul-Razzak, A. Nenes, Y. Ming, X. Liu, M. Ovchinnikov, B. Shipway, N. Meskhidze, J. Xu, and X. Shi (2011), Droplet nucleation: Physically-based parameterizations and comparative evaluation, *J. Adv. Model. Earth Syst.*, *3*(10), M10001.

Hudson, J. G., and S. Mishra (2007), Relationships between CCN and cloud microphysics variations in clean maritime air, *Geophys. Res. Lett.*, *34*(16), L16804.

Kirshbaum, D. J., and R. B. Smith (2009), Orographic Precipitation in the Tropics: Large-Eddy Simulations and Theory, *J. Atmos. Sci.*, *66*, 2259-2578.

Liu, Y., and P. H. Daum (2000), The effect of refractive index on size distributions and light scattering coefficients derived from optical particle counters, *Journal of Aerosol Science*, *31*(8), 945-957.

Lohmann, U., and J. Feichter (2005), Global indirect aerosol effects: a review, *Atmos. Chem. Phys.*, *5*, 715-737.

Morrison, H., and A. Gettelman (2008), A New Two-Moment Bulk Stratiform Cloud Microphysics Scheme in the Community Atmosphere Model, Version 3 (CAM3). Part I: Description and Numerical Tests, *Journal of Climate*, *21*(15), 3642-3659.

Nenes, A., S. Ghan, H. Abdul-Razzak, P. Y. Chuang, and J. H. Seinfeld (2001), Kinetic limitations on cloud droplet formation and impact on cloud albedo, *Tellus B*, *53*(2), 133-149.

Peter, J. R., A. M. Blyth, B. Brooks, J. B. McQuaid, J. J. N. Lingard, and M. H. Smith (2008), On the composition of Caribbean maritime aerosol particles measured during RICO, *Quarterly Journal of the Royal Meteorological Society*, *134*(633), 1059-1063.

Ramaswamy, V., O. Boucher, J. Haigh, D. Hauglustaine, J. Haywood, G. Myhre, T. Nakajima, G. Shi, and S. Solomon (2001), Radiative Forcing of Climate Change, in *Climate Change 2001: The Scientific Basis. Contribution of Working Group I to the Third Assessment Report of the Intergovernmental Panel on Climate Change.* , edited by J. T. Houghton, Y. Ding, D. J. Griggs, M. Noguer, P. J. van der Linden, X. Dai, K. Maskell and C. A. Johnson, pp. 349-416, Cambridge University Press, Cambridge, United Kingdom and New York, NY, USA.

Seinfeld, J. H., and S. N. Pandis (2006), *Atmospheric Chemistry and Physics: From Air Pollution to Climate Change, Second Edition*, John Wiley and Sons, New York.

Seland, Ø., T. Iversen, A. L. F. Kirkevåg, and T. Storelvmo (2008), Aerosol-climate interactions in the CAM-Oslo atmospheric GCM and investigation of associated basic shortcomings, *Tellus A*, *60*(3), 459-491.

Smith, R. B., A. Nugent, J. Minder, D. Kirshbaum, R. Warren, N. Lareau, P. Palany, A. James, and J. French (2012), Orographic Precipitation in the Tropics: The Dominica Experiment, *B. Am. Meteorol. Soc.*

Weast, R. C. (1987), Physical constants of organic compounds, in *CRC Handbook of Chemistry and Physics, 68th ed.*, edited by R. C. Weast, pp. B67-B146, CRC Press, Boca Raton, FL.

Woodcock, A. H. (1960), The Origin of Trade-Wind Orographic Shower Rains, *Tellus*, *12*(3), 315-326.

Appendix A: PCASP Size Bins

Bin number	Lower size bound (μm)	Upper size bound (μm)
1	0.0950	0.1050
2	0.1050	0.1150
3	0.1150	0.1250
4	0.1250	0.1350
5	0.1350	0.1420
6	0.1420	0.1520
7	0.1520	0.1620
8	0.1620	0.1720
9	0.1720	0.1920
10	0.1920	0.2120
11	0.2120	0.2320
12	0.2320	0.2520
13	0.2520	0.2720
14	0.2720	0.2920
15	0.2920	0.3910

Bin number	Lower size bound (μm)	Upper size bound (μm)
16	0.3910	0.4910
17	0.4910	0.5910
18	0.5910	0.6910
19	0.6910	0.7910
20	0.7910	0.8910
21	0.8910	0.9910
22	0.9910	1.1910
23	1.1910	1.3910
24	1.3910	1.5910
25	1.5910	1.7910
26	1.7910	1.9910
27	1.9910	2.2910
28	2.2910	2.5910
29	2.5910	2.9910

Appendix B: Details of Model Runs from Sensitivity Tests

(For the high wind standard run see Table 5, Section 5.1; for the low wind run see Table 12, Section 6.)

Table B1: T = 293 K run from temperature sensitivity test (section 5.1.2.1)

Assumptions common to all flights					
Mode composition:	Aitken mode	Ammonium sulfate (B = 0.507)			
	accumulation mode	Ammonium sulfate (B = 0.507)			
	coarse mode	Sea salt (NaCl) (B = 1.15)			
	giant mode	Sea salt (NaCl) (B = 1.15)			
Source air for aerosols		Average of Legs 1L and 1H			
Leg for cloud penetrations		Leg 3			
LWC criterion for cloud penetrations		0.25 g m^{-3}			
Cloud base temperature, T		293 K			
Cloud base air density, ρ_{air}		0.001275 g cm^{-3}			
Aitken mode median diameter, $a_{m,A}$ (µm)		0.0400			
Aitken mode geometric standard deviation, σ_A		1.5900			
Parameters obtained for specific flights					
Flight		RF12	RF13	RF16	RF17
Aitken mode number concentration, $N_{t,A}$ (cm^{-3})		309.1659	188.7157	194.2078	242.1256
accumulation mode:	med. diam., $a_{m,ac}$ (µm)	0.16748	0.17326	0.17391	0.16956
	geom. st. dev., σ_{ac}	1.3346	1.3238	1.3230	1.3175
	# conc., $N_{t,ac}$ (cm^{-3})	63.0903	73.6958	44.1049	71.0363
coarse mode:	med. diam., $a_{m,c}$ (µm)	0.69727	0.69025	0.69237	0.69875
	geom. st. dev., σ_c	1.3653	1.3472	1.2210	1.2703
	# conc., $N_{t,c}$ (cm^{-3})	2.1259	2.0310	0.80399	1.3025
giant mode:	med. diam., $a_{m,g}$ (µm)	1.7398	1.6900	1.4996	1.6917
	geom. st. dev., σ_g	1.3333	1.2822	1.2684	1.2801
	# conc., $N_{t,g}$ (cm^{-3})	0.12616	0.13346	0.060162	0.10349
Mean in-cloud updraft velocity, $\overline{w}$ (m/s)		1.6260	1.1317	0.97668	0.8012
St. dev. in-cloud updraft velocity, σ_w (m/s)		2.2442	1.8845	1.3330	1.9819
Model results					
Maximum supersaturation, S_{max}		0.014949	0.013784	0.012931	0.013451
Activation fraction:	Aitken mode	0.341595	0.289550	0.304496	0.254080
	accumulation mode	0.756564	0.716213	0.759516	0.647975
	coarse mode	0.764735	0.725438	0.767356	0.657067
	giant mode	0.764831	0.725566	0.767429	0.657166
Max. theoretical activation fraction		0.765631	0.725923	0.768127	0.656989
Droplet concentration: (cm^{-3})	Aitken mode	105.6095	54.64255	59.13546	61.51919
	accumulation mode	47.73186	52.7819	33.49836	46.02977
	coarse mode	1.62575	1.473364	0.616947	0.855830
	giant mode	9.65E-02	9.68E-02	4.62E-02	6.80E-02
	total	**155.0636**	**108.9946**	**93.29694**	**108.4728**
Droplet observations					
Observed droplet conc.:	CDP (cm^{-3})	**88.1252**	**90.6758**	**64.6817**	**74.9966**
Observed droplet conc.:	FSSP (cm^{-3})	**90.3395**	**95.0190**	**71.9676**	**82.4292**

Table B2: minus 0.5 m/s run from $\overline{w}$ sensitivity test (section 5.1.2.2)					
Assumptions common to all flights					
Mode composition:	Aitken mode	Ammonium sulfate (B = 0.507)			
	accumulation mode	Ammonium sulfate (B = 0.507)			
	coarse mode	Sea salt (NaCl) (B = 1.15)			
	giant mode	Sea salt (NaCl) (B = 1.15)			
Source air for aerosols		Average of Legs 1L and 1H			
Leg for cloud penetrations		Leg 3			
LWC criterion for cloud penetrations		0.25 g m^{-3}			
Cloud base temperature, T		300 K			
Cloud base air density, ρ_{air}		0.001275 g cm^{-3}			
Aitken mode median diameter, $a_{m,A}$ (µm)		0.0400			
Aitken mode geometric standard deviation, σ_A		1.5900			
Parameters obtained for specific flights					
Flight		RF12	RF13	RF16	RF17
Aitken mode number concentration, $N_{t,A}$ (cm^{-3})		309.1659	188.7157	194.2078	242.1256
accumulation mode:	med. diam., $a_{m,ac}$ (µm)	0.16748	0.17326	0.17391	0.16956
	geom. st. dev., σ_{ac}	1.3346	1.3238	1.3230	1.3175
	# conc., $N_{t,ac}$ (cm^{-3})	63.0903	73.6958	44.1049	71.0363
coarse mode:	med. diam., $a_{m,c}$ (µm)	0.69727	0.69025	0.69237	0.69875
	geom. st. dev., σ_c	1.3653	1.3472	1.2210	1.2703
	# conc., $N_{t,c}$ (cm^{-3})	2.1259	2.0310	0.80399	1.3025
giant mode:	med. diam., $a_{m,g}$ (µm)	1.7398	1.6900	1.4996	1.6917
	geom. st. dev., σ_g	1.3333	1.2822	1.2684	1.2801
	# conc., $N_{t,g}$ (cm^{-3})	0.12616	0.13346	0.060162	0.10349
Mean in-cloud updraft velocity, $\overline{w}$ (m/s)		1.1260	0.6317	0.47668	0.3012
St. dev. in-cloud updraft velocity, σ_w (m/s)		2.2442	1.8845	1.3330	1.9819
Model results					
Maximum supersaturation, S_{max}		0.012838	0.011813	0.011075	0.011472
Activation fraction:	Aitken mode	0.263385	0.208736	0.200553	0.180677
	accumulation mode	0.681291	0.619808	0.629093	0.550127
	coarse mode	0.691820	0.631490	0.639952	0.561108
	giant mode	0.691937	0.631643	0.640047	0.561219
Max. theoretical activation fraction		0.692074	0.631266	0.639678	0.560397
Droplet concentration: (cm^{-3})	Aitken mode	81.42968	39.39176	38.94904	43.7466
	accumulation mode	42.98283	45.67726	27.74609	39.07901
	coarse mode	1.470741	1.282557	0.514515	0.730843
	giant mode	8.73E-02	8.43E-02	3.85E-02	5.81E-02
	total	**125.9706**	**86.43588**	**67.24815**	**83.61454**
Droplet observations					
Observed droplet conc.: CDP (cm^{-3})		**88.1252**	**90.6758**	**64.6817**	**74.9966**
Observed droplet conc.: FSSP (cm^{-3})		**90.3395**	**95.0190**	**71.9676**	**82.4292**

Table B3: plus 0.5 m/s run from $\overline{w}$ sensitivity test (section 5.1.2.2)					
Assumptions common to all flights					
Mode composition:	Aitken mode	Ammonium sulfate (B = 0.507)			
	accumulation mode	Ammonium sulfate (B = 0.507)			
	coarse mode	Sea salt (NaCl) (B = 1.15)			
	giant mode	Sea salt (NaCl) (B = 1.15)			
Source air for aerosols		Average of Legs 1L and 1H			
Leg for cloud penetrations		Leg 3			
LWC criterion for cloud penetrations		0.25 g m^{-3}			
Cloud base temperature, T		300 K			
Cloud base air density, ρ_{air}		0.001275 g cm^{-3}			
Aitken mode median diameter, $a_{m,A}$ (µm)		0.0400			
Aitken mode geometric standard deviation, σ_A		1.5900			
Parameters obtained for specific flights					
Flight		RF12	RF13	RF16	RF17
Aitken mode number concentration, $N_{t,A}$ (cm^{-3})		309.1659	188.7157	194.2078	242.1256
accumulation mode:	med. diam., $a_{m,ac}$ (µm)	0.16748	0.17326	0.17391	0.16956
	geom. st. dev., σ_{ac}	1.3346	1.3238	1.3230	1.3175
	# conc., $N_{t,ac}$ (cm^{-3})	63.0903	73.6958	44.1049	71.0363
coarse mode:	med. diam., $a_{m,c}$ (µm)	0.69727	0.69025	0.69237	0.69875
	geom. st. dev., σ_c	1.3653	1.3472	1.2210	1.2703
	# conc., $N_{t,c}$ (cm^{-3})	2.1259	2.0310	0.80399	1.3025
giant mode:	med. diam., $a_{m,g}$ (µm)	1.7398	1.6900	1.4996	1.6917
	geom. st. dev., σ_g	1.3333	1.2822	1.2684	1.2801
	# conc., $N_{t,g}$ (cm^{-3})	0.12616	0.13346	0.060162	0.10349
Mean in-cloud updraft velocity, $\overline{w}$ (m/s)		2.1260	1.6317	1.47668	1.3012
St. dev. in-cloud updraft velocity, σ_w (m/s)		2.2442	1.8845	1.3330	1.9819
Model results					
Maximum supersaturation, S_{max}		0.013419	0.012920	0.012613	0.012653
Activation fraction:	Aitken mode	0.369688	0.326857	0.362448	0.290060
	accumulation mode	0.818937	0.796925	0.858082	0.734562
	coarse mode	0.826675	0.805561	0.864501	0.743647
	giant mode	0.826759	0.805672	0.864556	0.743738
Max. theoretical activation fraction		0.828265	0.806715	0.866023	0.744262
Droplet concentration: (cm^{-3})	Aitken mode	114.2951	61.68305	70.39024	70.23105
	accumulation mode	51.66695	58.73003	37.84561	52.18059
	coarse mode	1.757429	1.636094	0.695050	0.968600
	giant mode	0.104304	0.107525	5.20E-02	7.70E-02
	total	**167.8238**	**122.1567**	**108.9829**	**123.4572**
Droplet observations					
Observed droplet conc.:	CDP (cm^{-3})	**88.1252**	**90.6758**	**64.6817**	**74.9966**
Observed droplet conc.:	FSSP (cm^{-3})	**90.3395**	**95.0190**	**71.9676**	**82.4292**

Table B4: $a_{m,A}$ = 0.044 μm run from Aitken mode median diameter sensitivity test (section 5.1.2.3)					
Assumptions common to all flights					
Mode composition:	Aitken mode	Ammonium sulfate (B = 0.507)			
	accumulation mode	Ammonium sulfate (B = 0.507)			
	coarse mode	Sea salt (NaCl) (B = 1.15)			
	giant mode	Sea salt (NaCl) (B = 1.15)			
Source air for aerosols		Average of Legs 1L and 1H			
Leg for cloud penetrations		Leg 3			
LWC criterion for cloud penetrations		0.25 g m^{-3}			
Cloud base temperature, T		300 K			
Cloud base air density, ρ_{air}		0.001275 g cm^{-3}			
Aitken mode median diameter, $a_{m,A}$ (μm)		0.0440			
Aitken mode geometric standard deviation, σ_A		1.5900			
Parameters obtained for specific flights					
Flight		RF12	RF13	RF16	RF17
Aitken mode number concentration, $N_{t,A}$ (cm^{-3})		314.5948	192.0296	197.6181	246.3773
accumulation mode:	med. diam., $a_{m,ac}$ (μm)	0.17103	0.17538	0.17708	0.17189
	geom. st. dev., σ_{ac}	1.3352	1.3167	1.3230	1.3175
	# conc., $N_{t,ac}$ (cm^{-3})	58.7378	70.7981	41.6666	67.6489
coarse mode:	med. diam., $a_{m,c}$ (μm)	0.69727	0.69025	0.69237	0.69875
	geom. st. dev., σ_c	1.3653	1.3472	1.2210	1.2703
	# conc., $N_{t,c}$ (cm^{-3})	2.1258	2.0310	0.80398	1.3025
giant mode:	med. diam., $a_{m,g}$ (μm)	1.7398	1.6900	1.4996	1.6917
	geom. st. dev., σ_g	1.3333	1.2822	1.2684	1.2801
	# conc., $N_{t,g}$ (cm^{-3})	0.12616	0.13346	0.060162	0.10349
Mean in-cloud updraft velocity, $\overline{w}$ (m/s)		1.6260	1.1317	0.97668	0.8012
St. dev. in-cloud updraft velocity, σ_w (m/s)		2.2442	1.8845	1.3330	1.9819
Model results					
Maximum supersaturation, S_{max}		0.013256	0.012260	0.011454	0.011936
Activation fraction:	Aitken mode	0.363564	0.310820	0.325804	0.272467
	accumulation mode	0.756114	0.715431	0.759013	0.647194
	coarse mode	0.764728	0.725430	0.767350	0.657061
	giant mode	0.764830	0.725565	0.767428	0.657165
Max. theoretical activation fraction		0.765631	0.725923	0.768127	0.656989
Droplet concentration: (cm^{-3})	Aitken mode	114.3752	59.68668	64.38481	67.12974
	accumulation mode	44.41245	50.65113	31.62551	43.78196
	coarse mode	1.625658	1.473348	0.616934	0.855821
	giant mode	9.65E-02	9.68E-02	4.62E-02	6.80E-02
	total	**160.5098**	**111.908**	**96.67343**	**111.8355**
Droplet observations					
Observed droplet conc.: CDP (cm^{-3})		**88.1252**	**90.6758**	**64.6817**	**74.9966**
Observed droplet conc.: FSSP (cm^{-3})		**90.3395**	**95.0190**	**71.9676**	**82.4292**

Table B5: $a_{m,A}$ = 0.036 µm run from Aitken mode median diameter sensitivity test (section 5.1.2.3)					
Assumptions common to all flights					
Mode composition:	Aitken mode	Ammonium sulfate (B = 0.507)			
	accumulation mode	Ammonium sulfate (B = 0.507)			
	coarse mode	Sea salt (NaCl) (B = 1.15)			
	giant mode	Sea salt (NaCl) (B = 1.15)			
Source air for aerosols		Average of Legs 1L and 1H			
Leg for cloud penetrations		Leg 3			
LWC criterion for cloud penetrations		0.25 g m^{-3}			
Cloud base temperature, T		300 K			
Cloud base air density, ρ_{air}		0.001275 g cm^{-3}			
Aitken mode median diameter, $a_{m,A}$ (µm)		0.0360			
Aitken mode geometric standard deviation, σ_A		1.5900			
Parameters obtained for specific flights					
Flight		RF12	RF13	RF16	RF17
Aitken mode number concentration, $N_{t,A}$ (cm^{-3})		305.5751	186.5239	191.9522	239.3135
accumulation mode:	med. diam., $a_{m,ac}$ (µm)	0.16409	0.17147	0.17060	0.16729
	geom. st. dev., σ_{ac}	1.3542	1.3299	1.3368	1.3248
	# conc., $N_{t,ac}$ (cm^{-3})	67.1356	76.1651	46.6460	74.2044
coarse mode:	med. diam., $a_{m,c}$ (µm)	0.69727	0.69025	0.69237	0.69875
	geom. st. dev., σ_c	1.3653	1.3472	1.2210	1.2703
	# conc., $N_{t,c}$ (cm^{-3})	2.1259	2.0310	0.8040	1.3025
giant mode:	med. diam., $a_{m,g}$ (µm)	1.7398	1.6900	1.4996	1.6917
	geom. st. dev., σ_g	1.3333	1.2822	1.2684	1.2801
	# conc., $N_{t,g}$ (cm^{-3})	0.12616	0.13346	0.060162	0.10349
Mean in-cloud updraft velocity, $\overline{w}$ (m/s)		1.6260	1.1317	0.97668	0.8012
St. dev. in-cloud updraft velocity, σ_w (m/s)		2.2442	1.8845	1.3330	1.9819
Model results					
Maximum supersaturation, S_{max}		0.013589	0.012499	0.011751	0.012215
Activation fraction:	Aitken mode	0.264399	0.218620	0.229243	0.191351
	accumulation mode	0.754816	0.714696	0.757672	0.646301
	coarse mode	0.764729	0.725429	0.767351	0.657061
	giant mode	0.764830	0.725565	0.767428	0.657165
Max. theoretical activation fraction		0.765631	0.725923	0.768127	0.656989
Droplet concentration: (cm^{-3})	Aitken mode	80.79361	40.77792	44.00377	45.793
	accumulation mode	50.67500	54.4349	35.34238	47.95837
	coarse mode	1.625737	1.473347	0.61695	0.855822
	giant mode	9.65E-02	9.68E-02	4.62E-02	6.80E-02
	total	**133.1908**	**96.783**	**80.00928**	**94.6752**
Droplet observations					
Observed droplet conc.: CDP (cm^{-3})		**88.1252**	**90.6758**	**64.6817**	**74.9966**
Observed droplet conc.: FSSP (cm^{-3})		**90.3395**	**95.0190**	**71.9676**	**82.4292**

Table B6: run of ARG model with 0.05 μm added to $a_{m,ac}$ for flights RF12, RF13, RF16, and RF17 (high wind cases)					
Assumptions common to all flights					
Mode composition:	Aitken mode	Ammonium sulfate (B = 0.507)			
	accumulation mode	Ammonium sulfate (B = 0.507)			
	coarse mode	Sea salt (NaCl) (B = 1.15)			
	giant mode	Sea salt (NaCl) (B = 1.15)			
Source air for aerosols		Average of Legs 1L and 1H			
Leg for cloud penetrations		Leg 3			
LWC criterion for cloud penetrations		0.25 g m^{-3}			
Cloud base temperature, T		300 K			
Cloud base air density, ρ_{air}		0.001275 g cm^{-3}			
Aitken mode median diameter, $a_{m,A}$ (μm)		0.0400			
Aitken mode geometric standard deviation, σ_A		1.5900			
Parameters obtained for specific flights					
Flight		RF12	RF13	RF16	RF17
Aitken mode number concentration, $N_{t,A}$ (cm^{-3})		309.1659	188.7157	194.2078	242.1256
accumulation mode:	med. diam., $a_{m,ac}$ (μm)	0.21748	0.22326	0.22391	0.21956
	geom. st. dev., σ_{ac}	1.3346	1.3238	1.3230	1.3175
	# conc., $N_{t,ac}$ (cm^{-3})	63.0903	73.6958	44.1049	71.0363
coarse mode:	med. diam., $a_{m,c}$ (μm)	0.69727	0.69025	0.69237	0.69875
	geom. st. dev., σ_c	1.3653	1.3472	1.2210	1.2703
	# conc., $N_{t,c}$ (cm^{-3})	2.1259	2.0310	0.80399	1.3025
giant mode:	med. diam., $a_{m,g}$ (μm)	1.7398	1.6900	1.4996	1.6917
	geom. st. dev., σ_g	1.3333	1.2822	1.2684	1.2801
	# conc., $N_{t,g}$ (cm^{-3})	0.12616	0.13346	0.060162	0.10349
Mean in-cloud updraft velocity, $\overline{w}$ (m/s)		1.6260	1.1317	0.97668	0.8012
St. dev. in-cloud updraft velocity, σ_w (m/s)		2.2442	1.8845	1.3330	1.9819
Model results					
Maximum supersaturation, S_{max}		0.012813	0.016885	0.011041	0.011423
Activation fraction:	Aitken mode	0.297985	0.245807	0.260247	0.215455
	accumulation mode	0.759740	0.719408	0.762378	0.651196
	coarse mode	0.764695	0.725375	0.767311	0.657010
	giant mode	0.764825	0.725556	0.767419	0.657156
Max. theoretical activation fraction		0.765631	0.725923	0.768127	0.656989
Droplet concentration: (cm^{-3})	Aitken mode	92.12665	46.38772	50.54207	52.16725
	accumulation mode	47.93225	53.01736	33.62462	46.25856
	coarse mode	1.625666	1.473238	0.61691	0.855756
	giant mode	9.65E-02	9.68E-02	4.62E-02	6.80E-02
	total	**141.7811**	**100.9751**	**84.82977**	**99.34957**
Droplet observations					
Observed droplet conc.: CDP (cm^{-3})		**88.1252**	**90.6758**	**64.6817**	**74.9966**
Observed droplet conc.: FSSP (cm^{-3})		**90.3395**	**95.0190**	**71.9676**	**82.4292**

Table B7: Run of ARG model with Leg 1L used as aerosol source air for flights RF12, RF13, RF16, and RF17 (high wind cases)

Assumptions common to all flights					
Mode composition:	Aitken mode	Ammonium sulfate (B = 0.507)			
	accumulation mode	Ammonium sulfate (B = 0.507)			
	coarse mode	Sea salt (NaCl) (B = 1.15)			
	giant mode	Sea salt (NaCl) (B = 1.15)			
Source air for aerosols		Leg 1L			
Leg for cloud penetrations		Leg 3			
LWC criterion for cloud penetrations		0.25 g m^{-3}			
Cloud base temperature, T		300 K			
Cloud base air density, ρ_{air}		0.001275 g cm^{-3}			
Aitken mode median diameter, $a_{m,A}$ (μm)		0.0400			
Aitken mode geometric standard deviation, σ_A		1.5900			
Parameters obtained for specific flights					
Flight		RF12	RF13	RF16	RF17
Aitken mode number concentration, $N_{t,A}$ (cm^{-3})		310.5029	208.1091	178.4382	260.2185
accumulation mode:	med. diam., $a_{m,ac}$ (μm)	0.16782	0.17224	0.17270	0.16839
	geom. st. dev., σ_{ac}	1.3406	1.3309	1.3217	1.3197
	# conc., $N_{t,ac}$ (cm^{-3})	68.6898	84.7451	64.9858	89.7139
coarse mode:	med. diam., $a_{m,c}$ (μm)	0.69103	0.68814	0.68965	0.69525
	geom. st. dev., σ_c	1.3646	1.3295	1.2252	1.2543
	# conc., $N_{t,c}$ (cm^{-3})	2.7895	2.7726	1.2413	1.8391
giant mode:	med. diam., $a_{m,g}$ (μm)	1.7214	1.6232	1.6344	1.6512
	geom. st. dev., σ_g	1.2682	1.2582	1.1987	1.1770
	# conc., $N_{t,g}$ (cm^{-3})	0.15499	0.18896	0.085576	0.13145
Mean in-cloud updraft velocity, $\overline{w}$ (m/s)		1.6260	1.1317	0.97668	0.8012
St. dev. in-cloud updraft velocity, σ_w (m/s)		2.2442	1.8845	1.3330	1.9819
Model results					
Maximum supersaturation, S_{max}		0.013021	0.011669	0.010757	0.012853
Activation fraction:	Aitken mode	0.304352	0.246430	0.251465	0.213235
	accumulation mode	0.754622	0.713038	0.755889	0.644649
	coarse mode	0.764706	0.725398	0.767310	0.657030
	giant mode	0.764828	0.725558	0.767426	0.657160
Max. theoretical activation fraction		0.765631	0.725923	0.768127	0.656989
Droplet concentration: (cm^{-3})	Aitken mode	94.50227	51.28436	44.87091	55.48765
	accumulation mode	51.83480	60.42646	49.12204	57.83396
	coarse mode	2.133149	2.011239	0.952461	1.208344
	giant mode	0.118541	0.137101	6.57E-02	8.64E-02
	total	**148.5888**	**113.8592**	**95.01109**	**114.6163**
Droplet observations					
Observed droplet conc.: CDP (cm^{-3})		**88.1252**	**90.6758**	**64.6817**	**74.9966**
Observed droplet conc.: FSSP (cm^{-3})		**90.3395**	**95.0190**	**71.9676**	**82.4292**

Table B8: Run of ARG model with Leg 1H used as aerosol source air for flights RF12, RF13, RF16, and RF17 (high wind cases)					
Assumptions common to all flights					
Mode composition:	Aitken mode	Ammonium sulfate (B = 0.507)			
	accumulation mode	Ammonium sulfate (B = 0.507)			
	coarse mode	Sea salt (NaCl) (B = 1.15)			
	giant mode	Sea salt (NaCl) (B = 1.15)			
Source air for aerosols		Leg 1H			
Leg for cloud penetrations		Leg 3			
LWC criterion for cloud penetrations		0.25 g m^{-3}			
Cloud base temperature, T		300 K			
Cloud base air density, ρ_{air}		0.001275 g cm^{-3}			
Aitken mode median diameter, $a_{m,A}$ (µm)		0.0400			
Aitken mode geometric standard deviation, σ_A		1.5900			
Parameters obtained for specific flights					
Flight		RF12	RF13	RF16	RF17
Aitken mode number concentration, $N_{t,A}$ (cm^{-3})		307.8288	169.3224	209.9774	224.0327
accumulation mode:	med. diam., $a_{m,ac}$ (µm)	0.16703	0.17467	0.17611	0.17171
	geom. st. dev., σ_{ac}	1.3496	1.3141	1.3327	1.3115
	# conc., $N_{t,ac}$ (cm^{-3})	57.4908	62.6466	23.6531	52.3587
coarse mode:	med. diam., $a_{m,c}$ (µm)	0.70896	0.69710	0.69914	0.70809
	geom. st. dev., σ_c	1.3687	1.3664	1.2105	1.5309
	# conc., $N_{t,c}$ (cm^{-3})	1.4622	1.2895	0.36664	0.76587
giant mode:	med. diam., $a_{m,g}$ (µm)	1.7662	1.8235	1.3359	2.5738
	geom. st. dev., σ_g	1.4161	1.2423	1.2609	1.1048
	# conc., $N_{t,g}$ (cm^{-3})	0.095813	0.083897	0.034639	0.0083026
Mean in-cloud updraft velocity, $\overline{w}$ (m/s)		1.6260	1.1317	0.97668	0.8012
St. dev. in-cloud updraft velocity, σ_w (m/s)		2.2442	1.8845	1.3330	1.9819
Model results					
Maximum supersaturation, S_{max}		0.013873	0.013263	0.012837	0.013220
Activation fraction:	Aitken mode	0.328788	0.289501	0.317269	0.260447
	accumulation mode	0.756346	0.717074	0.761106	0.649323
	coarse mode	0.764751	0.725464	0.767391	0.657064
	giant mode	0.764832	0.725573	0.767432	0.657174
Max. theoretical activation fraction		0.765631	0.725923	0.768127	0.656989
Droplet concentration: (cm^{-3})	Aitken mode	101.2105	49.01897	66.6194	58.34858
	accumulation mode	43.48294	44.92223	18.00252	33.99772
	coarse mode	1.118219	0.935485	0.281356	0.503226
	giant mode	7.33E-02	6.09E-02	2.66E-02	5.46E-03
	total	**145.8849**	**94.93756**	**84.92986**	**92.85499**
Droplet observations					
Observed droplet conc.: CDP (cm^{-3})		**88.1252**	**90.6758**	**64.6817**	**74.9966**
Observed droplet conc.: FSSP (cm^{-3})		**90.3395**	**95.0190**	**71.9676**	**82.4292**

Table B9: Run of ARG model, and observed cloud droplet concentrations, with LWC criterion of 0.30 g m^{-3} for cloud penetrations (high wind flights)

Assumptions common to all flights					
Mode composition:	Aitken mode	Ammonium sulfate (B = 0.507)			
	accumulation mode	Ammonium sulfate (B = 0.507)			
	coarse mode	Sea salt (NaCl) (B = 1.15)			
	giant mode	Sea salt (NaCl) (B = 1.15)			
Source air for aerosols		Average of Legs 1L and 1H			
Leg for cloud penetrations		Leg 3			
LWC criterion for cloud penetrations		0.30 g m^{-3}			
Cloud base temperature, T		300 K			
Cloud base air density, ρ_{air}		0.001275 g cm^{-3}			
Aitken mode median diameter, $a_{m,A}$ (μm)		0.0400			
Aitken mode geometric standard deviation, σ_A		1.5900			
Parameters obtained for specific flights					
Flight		RF12	RF13	RF16	RF17
Aitken mode number concentration, $N_{t,A}$ (cm^{-3})		309.1659	188.7157	194.2078	242.1256
accumulation mode:	med. diam., $a_{m,ac}$ (μm)	0.16748	0.17326	0.17391	0.16956
	geom. st. dev., σ_{ac}	1.3346	1.3238	1.3230	1.3175
	# conc., $N_{t,ac}$ (cm^{-3})	63.0903	73.6958	44.1049	71.0363
coarse mode:	med. diam., $a_{m,c}$ (μm)	0.69727	0.69025	0.69237	0.69875
	geom. st. dev., σ_c	1.3653	1.3472	1.2210	1.2703
	# conc., $N_{t,c}$ (cm^{-3})	2.1259	2.0310	0.80399	1.3025
giant mode:	med. diam., $a_{m,g}$ (μm)	1.7398	1.6900	1.4996	1.6917
	geom. st. dev., σ_g	1.3333	1.2822	1.2684	1.2801
	# conc., $N_{t,g}$ (cm^{-3})	0.12616	0.13346	0.060162	0.10349
Mean in-cloud updraft velocity, $\overline{w}$ (m/s)		1.8077	1.1864	1.1125	0.8760
St. dev. in-cloud updraft velocity, σ_w (m/s)		2.2187	1.8977	1.3848	1.9959
Model results					
Maximum supersaturation, S_{max}		0.013347	0.012415	0.012331	0.012111
Activation fraction:	Aitken mode	0.335297	0.272855	0.302262	0.241762
	accumulation mode	0.782482	0.723327	0.779982	0.659498
	coarse mode	0.791242	0.73351	0.788160	0.669596
	giant mode	0.791338	0.733642	0.788230	0.669698
Max. theoretical activation fraction		0.792394	0.734072	0.789118	0.669632
Droplet concentration: (cm^{-3})	Aitken mode	103.6623	51.49200	58.70164	58.53684
	accumulation mode	49.36701	53.30615	34.40102	46.84828
	coarse mode	1.682102	1.489758	0.633673	0.872149
	giant mode	9.98E-02	9.79E-02	4.74E-02	6.93E-02
	total	**154.8112**	**106.3858**	**93.78375**	**106.3266**
Droplet observations					
Observed droplet conc.: CDP (cm^{-3})		**91.4388**	**93.6180**	**67.5774**	**77.1107**
Observed droplet conc.: FSSP (cm^{-3})		**94.0158**	**97.9148**	**75.4935**	**84.7854**

Table B10: Run of ARG model, and observed cloud droplet concentrations, with LWC criterion of 0.40 g m^{-3} for cloud penetrations (high wind flights)					
Assumptions common to all flights					
Mode composition:	Aitken mode	Ammonium sulfate (B = 0.507)			
	accumulation mode	Ammonium sulfate (B = 0.507)			
	coarse mode	Sea salt (NaCl) (B = 1.15)			
	giant mode	Sea salt (NaCl) (B = 1.15)			
Source air for aerosols		Average of Legs 1L and 1H			
Leg for cloud penetrations		Leg 3			
LWC criterion for cloud penetrations		0.40 g m^{-3}			
Cloud base temperature, T		300 K			
Cloud base air density, ρ_{air}		0.001275 g cm^{-3}			
Aitken mode median diameter, $a_{m,A}$ (μm)		0.0400			
Aitken mode geometric standard deviation, σ_A		1.5900			
Parameters obtained for specific flights					
Flight		RF12	RF13	RF16	RF17
Aitken mode number concentration, $N_{t,A}$ (cm^{-3})		309.1659	188.7157	194.2078	242.1256
accumulation mode:	med. diam., $a_{m,ac}$ (μm)	0.16748	0.17326	0.17391	0.16956
	geom. st. dev., σ_{ac}	1.3346	1.3238	1.3230	1.3175
	# conc., $N_{t,ac}$ (cm^{-3})	63.0903	73.6958	44.1049	71.0363
coarse mode:	med. diam., $a_{m,c}$ (μm)	0.69727	0.69025	0.69237	0.69875
	geom. st. dev., σ_c	1.3653	1.3472	1.2210	1.2703
	# conc., $N_{t,c}$ (cm^{-3})	2.1259	2.0310	0.80399	1.3025
giant mode:	med. diam., $a_{m,g}$ (μm)	1.7398	1.6900	1.4996	1.6917
	geom. st. dev., σ_g	1.3333	1.2822	1.2684	1.2801
	# conc., $N_{t,g}$ (cm^{-3})	0.12616	0.13346	0.060162	0.10349
Mean in-cloud updraft velocity, $\overline{w}$ (m/s)		2.2147	1.3657	1.3851	1.0535
St. dev. in-cloud updraft velocity, σ_w (m/s)		2.3304	1.8669	1.3871	1.9660
Model results					
Maximum supersaturation, S_{max}		0.014235	0.012325	0.012340	0.012607
Activation fraction:	Aitken mode	0.378622	0.293885	0.346793	0.260922
	accumulation mode	0.819858	0.757242	0.832688	0.693903
	coarse mode	0.827282	0.766907	0.839577	0.703711
	giant mode	0.827363	0.767032	0.839636	0.703810
Max. theoretical activation fraction		0.829033	0.767773	0.840995	0.703972
Droplet concentration: (cm^{-3})	Aitken mode	117.0570	55.4608	67.34988	63.17588
	accumulation mode	51.72511	55.80555	36.72561	49.29231
	coarse mode	1.758719	1.557589	0.675011	0.916584
	giant mode	0.104380	0.102368	5.05E-02	7.28E-02
	total	**170.6452**	**112.9263**	**104.8010**	**113.4576**
Droplet observations					
Observed droplet conc.: CDP (cm^{-3})		**101.1052**	**97.4155**	**73.5488**	**80.3381**
Observed droplet conc.: FSSP (cm^{-3})		**104.3182**	**102.276**	**81.5110**	**87.4960**

Table B11: Run of ARG model, and observed cloud droplet concentrations, with LWC criterion of 0.50 g m^{-3} for cloud penetrations (high wind flights)					
Assumptions common to all flights					
Mode composition:	Aitken mode	Ammonium sulfate (B = 0.507)			
	accumulation mode	Ammonium sulfate (B = 0.507)			
	coarse mode	Sea salt (NaCl) (B = 1.15)			
	giant mode	Sea salt (NaCl) (B = 1.15)			
Source air for aerosols		Average of Legs 1L and 1H			
Leg for cloud penetrations		Leg 3			
LWC criterion for cloud penetrations		0.50 g m^{-3}			
Cloud base temperature, T		300 K			
Cloud base air density, ρ_{air}		0.001275 g cm^{-3}			
Aitken mode median diameter, $a_{m,A}$ (µm)		0.0400			
Aitken mode geometric standard deviation, σ_A		1.5900			
Parameters obtained for specific flights					
Flight		RF12	RF13	RF16	RF17
Aitken mode number concentration, $N_{t,A}$ (cm^{-3})		309.1659	188.7157	194.2078	242.1256
accumulation mode:	med. diam., $a_{m,ac}$ (µm)	0.16748	0.17326	0.17391	0.16956
	geom. st. dev., σ_{ac}	1.3346	1.3238	1.3230	1.3175
	# conc., $N_{t,ac}$ (cm^{-3})	63.0903	73.6958	44.1049	71.0363
coarse mode:	med. diam., $a_{m,c}$ (µm)	0.69727	0.69025	0.69237	0.69875
	geom. st. dev., σ_c	1.3653	1.3472	1.2210	1.2703
	# conc., $N_{t,c}$ (cm^{-3})	2.1259	2.0310	0.80399	1.3025
giant mode:	med. diam., $a_{m,g}$ (µm)	1.7398	1.6900	1.4996	1.6917
	geom. st. dev., σ_g	1.3333	1.2822	1.2684	1.2801
	# conc., $N_{t,g}$ (cm^{-3})	0.12616	0.13346	0.060162	0.10349
Mean in-cloud updraft velocity, $\overline{w}$ (m/s)		2.8150	1.5203	1.6186	1.2607
St. dev. in-cloud updraft velocity, σ_w (m/s)		2.2537	1.8403	1.4019	1.9777
Model results					
Maximum supersaturation, S_{max}		0.014009	0.012782	0.012913	0.012641
Activation fraction:	Aitken mode	0.442536	0.312690	0.384662	0.285234
	accumulation mode	0.886067	0.785428	0.868441	0.728315
	coarse mode	0.891655	0.794567	0.874230	0.737527
	giant mode	0.891716	0.794685	0.874279	0.737620
Max. theoretical activation fraction		0.894177	0.795630	0.875867	0.738086
Droplet concentration: (cm^{-3})	Aitken mode	136.8172	59.00951	74.70441	69.06255
	accumulation mode	55.90221	57.88272	38.30252	51.73681
	coarse mode	1.89557	1.613765	0.702872	0.960630
	giant mode	0.112499	0.106059	5.26E-02	7.63E-02
	total	**194.7275**	**118.6121**	**113.7624**	**121.8363**
Droplet observations					
Observed droplet conc.:	CDP (cm^{-3})	**111.0791**	**103.0236**	**78.496**	**83.6832**
Observed droplet conc.:	FSSP (cm^{-3})	**116.1605**	**108.3799**	**86.794**	**91.5857**